A HYDRODYNAMIC THEORY OF HEAVY ION COLLISIONS

by

David Carl Mundinger

A THESIS

submitted to
Michigan State University
in partial fulfillment of the requirements
for the degree of

DOCTOR OF PHILOSOPHY

Department of Physics

1979

ABSTRACT

A HYDRODYNAMIC THEORY OF
HEAVY ION COLLISIONS

by

David Carl Mundinger

A macroscopic description of heavy ion collisions has been made based on the dynamics of an interacting Fermi liquid. This framework is general enough to permit the study of some of the bulk properties of the medium such as the stress tensor and the equation of state.

A computation was done, first of all, for the one-dimensional case using a Lagrangian technique. The breakup threshold was calculated for the collision between two semi-infinite slabs of nuclear matter. This one-dimensional model contains many of the features of heavy ion collisions. Based on these results a model was made for the collision between two spherical nuclei. The degrees of freedom that we emphasize are the centers of the two nuclei, and the location of two boundaries which separate the nuclear matter into a compressed region and two uncompressed regions. Using the equation of state, along with the conservation laws for mass and momentum, we can generate equations of motion for each

of the dynamical variables. The momentum transport between the two nuclei is taken from the theory of a collisionless Fermi gas.

Angular distributions, energy loss, and fusion cross-sections have been studied. Comparisons are made with experiment and with other models that have been suggested. Qualitatively the results are in accord with the more computer-intensive time dependent Hartree-Fock calculations.

TABLE OF CONTENTS

LIST OF TABLES

LIST OF FIGURES

Figure Page

CHAPTER I

INTRODUCTION

Machines with the capability of accelerating heavy ions up to energies on the order of 5-50 MeV/nucleon will soon be available. These energies represent a new domain of nuclear physics. The velocities are high enough to cause considerable interpenetration of the two nuclei, yet they are not so high that the system cannot respond collectively. It has been speculated that perhaps new kinds of phenomena will be observed.[1] It is important for us to gain theoretical understanding of how nuclear matter behaves in this situation. We recognize that a complete and detailed theory may be unachievable at this stage. However, based on what we do know about nuclear matter and based on experiments that have been done, various ideas have emerged. A number of attempts have been made at a theoretical description of heavy ion collisions. These theories are quite different from each other in the way they approach the problem. Several of the models will be described briefly here, and a more detailed account of the results will be presented later.

The most fundamental calculations are based on the time-dependent Hartree-Fock theory (TDHF). The theory starts from basic principles. The nucleus is visualized as a collection of quantum mechanical particles (nucleons) which interact via a two-body potential, usually a Coulomb plus a parametrized nuclear force. The nucleons are placed in states which are obtained in a self-consistent way from the mean field. As the system evolves, this procedure is repeated at each time step. These calculations have the obvious advantage of giving a detailed description of heavy ion collisions and should be able to predict such things as fusion cross-sections and other experimental observables. Much discussion and work in this area has appeared.[2,3,4,5,6] However, because the calculations are lengthy and consume much computer time, a detailed picture has not been presented. Results have been published for a few systems, usually at just one energy. Another problem with this theory is that it is unable to include two-body collisions. This will not be a serious problem at low energy but at higher energies two-body collisions will become increasingly important.

The simplest model to have emerged thus far has been that proposed by Gross and Kalinowski.[7] This is sometimes referred to as the classical friction model.

The number of degrees of freedom has been reduced drastically. Instead of following the nucleon coordinates as is done in the TDHF calculations, only the relative coordinates of the two nuclei are used to describe the system. A potential function is introduced which, along with the frictional force, governs the time development of the nuclear coordinates. This model offers a convenient picture of some of the more striking features of heavy ion collisions including fusion and large energy losses. It does not offer a very detailed description, and its usefulness is limited.

The classical irrotational fluid drop model has been the basis for several calculations concerning heavy ion collisions.[8,9] The goal has been to isolate those degrees of freedom which most completely describe the whole system. A smaller number of parameters means fewer equations of motion. Usually the surface is parametrized by surfaces of revolution, and collective variables such as the moments of the mass distribution are chosen to represent the nucleus. The potential energy can then be calculated from the configuration and the equations of motion solved numerically. For example, to study fusion one looks at the trajectory of the system in this multi-dimensional space. If the system enters a region where it gets trapped in a potential depression, one would say that the system is fused.

The fusion cross section as a function of energy has been calculated for several systems by Nix and Sierk.[8]

An entirely different approach is to isolate those collective quantum mechanical states which are most important in absorbing energy from the relative motion. This again reduces the number of equations that one must solve. In the range of energies associated with deeply inelastic collisions, surface excitations and giant resonances may be the dominant transitions. Calculations based on these ideas have been done for several nuclei by Broglia and co-workers.[10,11,12] Angular distributions, fusion cross sections, and deep inelastic energy losses have been studied.

This thesis will develop a hydrodynamic theory of collisions, based on the idea that the dynamics of nuclear matter can be represented by an equation of state. To begin with, a set of classical equations of motion will be derived from the microscopic ones. Following this the bulk properties of a fluid will be described. We also discuss some important macroscopic phenomena which will be useful in discussing heavy ion collisions within this theory. An equation of state will then be postulated based on the observed properties of nuclear matter. A model is constructed for the one-dimensional slab collision, and the results are

presented. This model is then generalized to describe a three-dimensional collision. The results of this calculation are to be compared with experimental data and the other models described above.

CHAPTER II

DERIVATION OF THE MACROSCOPIC EQUATIONS OF MOTION FROM A MICROSCOPIC THEORY

In setting down a theory of heavy ion collisions based on first principles, we will start with the description of each nucleus as a collection of nucleons which interact with each other according to the laws of quantum mechanics. There is a many-body wave function $\Psi(r_i, r_2, \ldots r_n; t)$ which depends on the nucleon coordinates and time, and obeys the Schrödinger equation,

$$i \frac{\partial}{\partial t} \Psi(r,t) = H\Psi(r,t). \tag{1}$$

This equation can be cast into a slightly different form by multiplying it by $\Psi^+(r't)$ on the left, then subtracting from this the equation obtained by taking the hermitian conjugate of (1), replacing r with r', and multiplying on the right by $\Psi(r,t)$. After rearranging terms and using the chain rule for differentiation, the result is

$$i \frac{\partial}{\partial t} (\Psi^+(r't)\Psi(r,t)) = \Psi^+ H\Psi - \Psi H\Psi^+$$

If we say that H' operates only on the primed coordinates and H only on the unprimed, then this equation can be written as

$$i \frac{\partial}{\partial t} N(r,r';t) = (H-H')N(r,r';t). \qquad (2)$$

This new quantity is called the N-body density matrix and is defined as

$$N(r,r';t) = \Psi^{+}(r',t)\Psi(r,t).$$

Its physical meaning is somewhat abstract, but useful quantities can be generated by integrating over the appropriate variables, as will be seen in the following discussion. The Hamiltonian H is an operator which represents the total energy,

$$H = \sum_{i=1}^{N} \frac{\tilde{P}_i^2}{2m} + \sum_{i<j}^{N} v(r_i r_j)$$

In configuration space H has the form

$$H = \sum_{i=1}^{N} \frac{-\nabla_i^2}{2m} + \sum_{i<j}^{N} v(r_i r_j)$$

$$H' = \sum_{i=1}^{N} \frac{-\nabla_i'^2}{2m} + \sum_{i<j}^{N} v(r_i' r_j').$$

By putting these expressions into Equation (2) we obtain directly the equation of motion for the N-body density matrix.[37]

$$i \frac{\partial}{\partial t} N(r,r';t) = \sum_{i=1}^{N} \frac{(\nabla_i^2 - \nabla_i'^2)}{2m} N(r,r';t)$$

$$+ \sum_{i<j}^{N} [v(r_i,r_j) - v(r_i',r_j')]N(r,r';t) \qquad (3)$$

Equation (3) is still very complicated and involves all the degrees of freedom twice. At this point, to make further progress, we adopt the following philosophy. In order to obtain a simpler expression we will give up the ability to describe the evolution of each degree of freedom and try to find a small set of variables which will describe the collective behavior of the system.[38] It is toward achieving this end that we define the n-body density matrix.

$$N^{(n)}(r_n,r_n';t) = \frac{N!}{(N-n)!} \int d^3r_p \Psi^+(r_n',r_p;t)\Psi(r_n,r_p;t) \qquad (4)$$

The coordinates $r_1 \ldots r_n$ are not integrated over. For the coordinates $r_{n+1} \ldots r_N$ we set $r_p = r_p'$ and integrate. With this definition a set of N equations can be written down. The nth equation is the equation of motion for

the n-body density matrix. To generate the nth equation divide the coordinates into two groups;

$$r_n = (r_1, r_2, \ldots r_n)$$

$$r_p = (r_{n+1}, \ldots r_N).$$

In Equation (3) set $r_p = r'_p$, multiply through by $\frac{N!}{(N-n)!}$, and integrate over all the coordinates r_p,

$$\int d^3 r_p \, \frac{N!}{(N-n)!} \, i\frac{\partial}{\partial t} \, N(r, r'_n r_p ; t)$$

$$= \int d^3 r_p \, \frac{N!}{(N-n)!} \sum_{i=1}^{N} \frac{(\nabla_i^2 - \nabla_i'^2)}{2m} \, N(r, r'_n r_p ; t)$$

$$+ \int d^3 r_p \sum_{i<j}^{N} [v(r_i r_j) - v(r'_i r'_j)] N(r, r'_n r_p ; t).$$

Evaluate this equation term by term. The left hand side is clearly just

$$i\frac{\partial}{\partial t} \, N^{(n)}(r_n, r'_n ; t).$$

In the first term on the right hand side if $i>n$ the integral vanishes. What remains is

$$-\sum_{i=1}^{N} \frac{(\nabla_i^2 - \nabla_i'^2)}{2m} \, N^{(n)}(r_n, r'_n ; t).$$

In the second term on the right hand side if both i and j are greater than n there is no contribution. If both i and j are less than or equal to n, the sum comes outside the integral giving

$$\sum_{i<j}^{n} [v(r_i r_j) - v(r_i' r_j')] N^{(n)}(r_n, r_n'; t).$$

If $i \leq n$ and $j > n$, the integral becomes

$$\int d^3 r_p [v(r_i r_j) - v(r_i' r_j)] N(r, r_n' r_j r_p; t)$$

where r_j is explicitly separated out of the set r_p. It is convenient to factor this integral as follows,

$$\int d^3 r_j [v(r_i r_j) - v(r_i' r_j)] \int d^3 r_p N(r, r_n' r_p'; t)$$

There will be an identical contribution for each j in the range $n < j \leq N$ giving a factor of $(N-n)$. Putting the appropriate prefactor in gives

$$\int d^3 r_j [v(r_i r_j) - v(r_i' r_j)] N^{(n+1)}(r_n r_j, r_n' r_j; t).$$

Finally, putting these pieces together, we can write the equation of motion for the n-body density matrix.

$$i\frac{\partial}{\partial t} N^{(n)}(r_n,r_n';t) = -\sum_{i=1}^{N} \frac{(\nabla_i^2-\nabla_i^2)}{2m} N^{(n)}(r_n,r_n';t)$$

$$+ \sum_{i<j}^{n} [v(r_i r_j) - v(r_i' r_j')] N^{(n)}(r_n,r_n';t)$$

$$+ \sum_{i=1}^{n} \int d^3 r_j [v(r_i r_j') - v(r_i' r_j)] N^{(n+1)}(r_n r_j, r_n' r_j;t) \qquad (5)$$

This equation expresses the time rate of change of the n-body density matrix in terms of the space derivitives, the two-body interaction, and the (n+1)-body density matrix. If we are to obtain a closed set of equations we must find an approximate expression for $N^{(n+1)}$ in terms of $N^{(n)}$, $N^{(n-1)}$,...$N^{(1)}$. This can be done if we take $\Psi(r,t)$ to be a Slater determinant wave function. After separating out the time we can write

$$\Psi(r) = \frac{1}{\sqrt{N!}} \sum_{P} (-1)^P [\phi_{p_1}(r_1)\phi_{p_2}(r_2)\ldots\phi_{p_3}(r_3)]. \qquad (6)$$

$\phi_{p_1}(r_i)$ are normalized single particle states and the sum over p represents a sum over all permutations.[40] Putting this expression back into Equation (4) we can generate a relationship between $N^{(n+1)}(r_n r_j, r_n' r_j)$ and the lower order density matrices. For the two-body case we get

$$N^{(2)}(r_1r_2,r_1'r_2') = N^{(1)}(r_1,r_1)N^{(1)}(r_2,r_2')$$

$$- N^{(1)}(r_1,r_2')N^{(1)}(r_2,r_1') \tag{7}$$

From this point on the discussion will be limited to the one-body equation and the superscripts will be omitted. We can now derive a closed expression for $N(r_1,r_1';t)$. (The explicit time dependence has been omitted.)

$$i\frac{\partial}{\partial t} N(r_1,r_1') = \frac{-(\nabla_1^2-\nabla_1'^2)}{2m} N(r_1,r_1')$$

$$+\int d^3r_2[v(r_1r_2) - v(r_1'r_2)]\ [N(r_1,r_1')N(r_2r_,_2)$$

$$- N(r_1r_2)N(r_2r_1')] \tag{8}$$

In this part of the discussion we will demonstrate how several quantities can be formed which can be interpreted physically. First of all look at the one-body density matrix.

$$N(r_1,r_1';t) = \sum_\alpha \phi_\alpha^*(r_1',t)\phi_\alpha(r_1,t)$$

If $r_1 = r_1'$ this is the ordinary density $\rho(r_1,t)$. If the operator $\frac{(\nabla_1-\nabla_1')}{2mi}$ acts on $N(r_1,r_1';t)$ before setting $r_1 = r_1'$, the current density vector is obtained.

$$\frac{(\nabla_1-\nabla_1')}{2mi}\sum_\alpha \phi_\alpha^*(r_1',t)\,\phi_\alpha(r_1,t)$$

$$= \frac{1}{2mi}\sum_\alpha [\phi_\alpha{}^*\nabla_1\phi_\alpha - \phi_\alpha\nabla_1\phi_\alpha^*] = \vec{J}(r_1,t)$$

By a similar operation a tensor quantity can be formed with units of a momentum flux density,

$$[\frac{(\nabla_1-\nabla_1')_i}{2i}\,\frac{(\nabla_1-\nabla_1')_j}{2mi}\,N(r_1,r_1';t)]_{r_1=r_1'} = T_{ij}(r_1,t).$$

If $\phi_\alpha(r)$ is interpreted as a probability amplitude then it is consistent to identify these quantities with their classical counterparts. Using these relations it is straightforward to show that

$$[(\nabla_1+\nabla_1')\cdot\frac{(\nabla_1-\nabla_1')}{2mi}\,N(r_1,r_1';t)]_{r_1=r_1'} = \nabla_r\cdot J(r,t),$$

and

$$[(\nabla_1+\nabla_1')_j\frac{(\nabla_1-\nabla_1')}{2i}{}_i\frac{(\nabla_1-\nabla_1')}{2mi}{}_j N(r_1,r_1';t)]_{r_1=r_1'}$$

$$= \frac{\partial}{\partial r_j}\,T_{ij}(r_1,t).$$

The fact that $N(r_1,r_1';t)$ is a function of two coordinates makes it somewhat inconvenient to visualize in physical terms. It would be more intuitive perhaps to have a phase space function. This was introduced by Wigner[13] and is known as the Wigner function.

$$f(r,p) = \int \frac{d^3x}{(2\pi)^3} e^{-ip\cdot x} N(r + \frac{x}{2}, r - \frac{x}{2})$$

Here we have defined relative and center of mass coordinates

$$\vec{x} = (\vec{r}_1 - \vec{r}_1')$$

$$\vec{r} = \tfrac{1}{2}(\vec{r}_1 + \vec{r}_1')$$

The derivitive operators are also related,

$$\nabla_1 = \tfrac{1}{2}\nabla_r + \nabla_x \qquad \nabla_1' = \tfrac{1}{2}\nabla_r - \nabla_x$$

$$\nabla_r = \nabla_1 + \nabla_1' \qquad \nabla_x = \tfrac{1}{2}(\nabla_1 - \nabla_1')$$

Evaluating the integrals of $f(r,p)d^3p$ will give additional physical insight.

$$\int f(r,p)d^3p = \int d^3x N(r + x/2, r - x/2) \int \frac{d^3p}{(2\pi)^3} e^{-ip\cdot x}$$

$$= \rho(r)$$

$$\int \vec{p} f(r,p)d^3p = \int d^3x N(r + x/2, r - x/2) i\nabla_x \delta(x)$$

$$= [m \frac{(\nabla_1 - \nabla_1')}{2mi} N(r_1, r_1')]_{r_1 = r_1'} = m\vec{J}(r)$$

$$\int \frac{p_i p_j}{m} f(r,p)d^3p = \int d^3x N(r + x/2, r - x/2) \times$$

$$\int \frac{d^3p}{(2\pi)^3} p_i p_j e^{-ip\cdot x}$$

$$= [\frac{(\nabla_1 - \nabla_1')}{2i} i \frac{(\nabla_1 - \nabla_1')}{2mi} j N(r_1, r_1')]_{r_1 = r_1'} = T_{ij}(r)$$

These integrals suggest that $f(r,p)$ be interpreted as a phase space distribution function.

Equation (8) still contains the integral over a product of one-body density matrices. The direct term contains $N(r_2,r_2)$ which is just $\rho(r_2)$. This can be simplified if we define an equivalent one body potential.

$$U(r_1) = \int d^3r_2 \; v(r_1r_2)\rho(r_2)$$

The direct interaction term becomes

$$N(r_1,r_1')[U_d(r_1) - U_d(r_1')].$$

The exchange term is more involved since it involves two density matrices.

$$\int d^3r_2 \; v(r_1r_2) \; N(r_1r_2)N(r_2r_1') \tag{9}$$

This, as it stands, is not a local one-body potential. An approximation can be made which will keep the equivalent one-body potential local.[14] Expand $N(r_2,r_1')$ about the point $r_2 = r_1$.

$$N(r_2,r_1') = N(r_1,r_1') + N(r_1,r_1')\cdot(r_2 - r_1)$$

$$+ \tfrac{1}{2}\nabla_i\nabla_j N(r_1,r_1') \times (r_2 - r_1)_i(r_2 - r_1)_j + \ldots$$

To the next lower approximation we can think of the nucleus as an infinite Fermi gas, in which case $N(r_1,r_2)$ is known explicitly.

$$N_{FG}(r_1,r_2) = \frac{1}{k_F|r_1-r_2|}\, j_1(k_F|r_1-r_2|)\,\rho\left(\frac{r_1+r_2}{2}\right)$$

With these approximations expression (9) becomes

$$N(r_1,r_1') \int d^3r_2 v(r_1 r_2) N_{FG}(r_1,r_2)$$

$$+ \nabla_j N(r_1,r_1') \int d^3r_2 (r_2-r_1)_j \; v(r_2 r_1) N_{FG}(r_2,r_1)$$

$$+ \nabla_i \nabla_j N(r_1,r_1') \int d^3r_2 (r_2-r_1)_j \; v(r_2,r_1) N_{FG}(r_2,r_1)$$

From the first term we can define an effective one-body potential which can be combined with the direct term to give a total effective one-body potential. The second term vanishes in the infinite Fermi gas limit, as do the cross terms in the third part. The third term contributes a ∇^2 which can be combined with the kinetic energy term to give an effective mass. Experimentally it is observed that the effective mass ratio is not much different from 1,[43] so, for purposes of this theory, only the first part of the exchange term will be used. It is combined with the direct term to give

$$N(r_1,r_1')[U(r_1) - U(r_1')].$$

Expressed in the relative and center-of-mass coordinates this becomes

$$N(r + x/2,\ r - x/2)[U(r + x/2) - U(r - x/2)].$$

If we now make the semi-classical approximation that U(r) varies slowly over the nucleus, then the interaction term becomes

$$N(r + x/2,\ r - x/2)x\cdot\nabla_r U(r).$$

The equation of motion (8) is now expressed in terms of a local one-body potential.

$$i\frac{\partial}{\partial t} N(r_1,r_1') = \frac{(\nabla_1^2-\nabla_1'^2)}{2m} N(r_1,r_1')$$

$$+ [(r_1-r_1')\cdot(\nabla_1+\nabla_1')U(\frac{r_1+r_1'}{2})]N(r_1,r_1') \qquad (10)$$

In the limit where $r_1 = r_1'$ the continuity equation is recovered,

$$\frac{\partial\rho}{\partial t} + \nabla_r\cdot\vec{J}(r,t) = 0 \qquad (11)$$

If we operate first on the left with $\tilde{P}_{rel} = i(\nabla_1-\nabla_1')_i$ and then set $r_1 = r_1'$ we will get another convervation law.

$$\frac{\partial}{\partial t}\ (mJ_i(r,t)) = -\frac{\partial}{\partial r_j}\ (T_{ij})$$

$$-\frac{\partial}{\partial x_i}\ [x_j\frac{\partial}{\partial r_j} U(r)N(r + x/2,\ r - x/2)]$$

$$m\frac{\partial}{\partial t}\vec{J}(r,t) + \frac{\partial}{\partial r_j}\ [T_{ij} + \delta_{ij}(\rho U-V)] = 0$$

where $\frac{\partial V}{\partial\rho} = U.$ (12)

This is the equation of momentum conservation. If we define a stress tensor P_{ij} as,

$$T_{ij} + \delta_{ij}(pU-V) = P_{ij} + m\rho u_i u_j$$

and combine Equations (12) and (11) we get Euler's equation of motion,

$$\rho\frac{\partial u}{\partial t} + \rho\vec{u}\cdot\nabla\vec{u} + \nabla\cdot\vec{\vec{P}} = 0.$$

The Fourier transform of Equation (10) is the equation of motion for the phase space distribution function.

$$\frac{\partial}{\partial t} f(r,p) + \frac{p}{m}\cdot\nabla_r f(r,p) - \nabla_r U\cdot\nabla_p f(r,p) = 0 \qquad (13)$$

This is the Vlasov equation.[15] It is just what one would write down for a classical system of particles if there were no collisions. Expressed in words, the change in each coordinate is given by the velocity associated with that coordinate, and the change in the velocity is proportional to the force.

The validity of Equation (13) rests on the introduction of a local one-body potential. The potential, which will depend on the density, is a fundamental quantity which must be chosen properly.

CHAPTER III

BULK PROPERTIES AND MACROSCOPIC PHENOMENA

In this section we will first discuss some of the bulk properties of a general fluid. Then several examples will be presented which illustrate the different kinds of macroscopic behavior. Consider an ordinary fluid whose energy is known as a function of density. A typical energy-density curve is shown in Figure 1. Assuming that the fluid has an isotropic stress tensor, which is the case for most normal fluids, we can define a pressure which is also a function of the density.

$$P = -\frac{\partial E}{\partial V} = \rho^2 \frac{\partial (E/n)}{\partial \rho}$$

At equilibrium density the energy function will have a minimum. The pressure at this point will be zero. Another important property of a fluid is its compressibility. This is related to the second derivative of the energy function.

$$k = -V\frac{\partial P}{\partial V}\Big|_{\rho_0} = \frac{\partial P}{\partial \rho}\Big|_{\rho_0}$$

A convention often used in nuclear physics is to define the compressibility K,

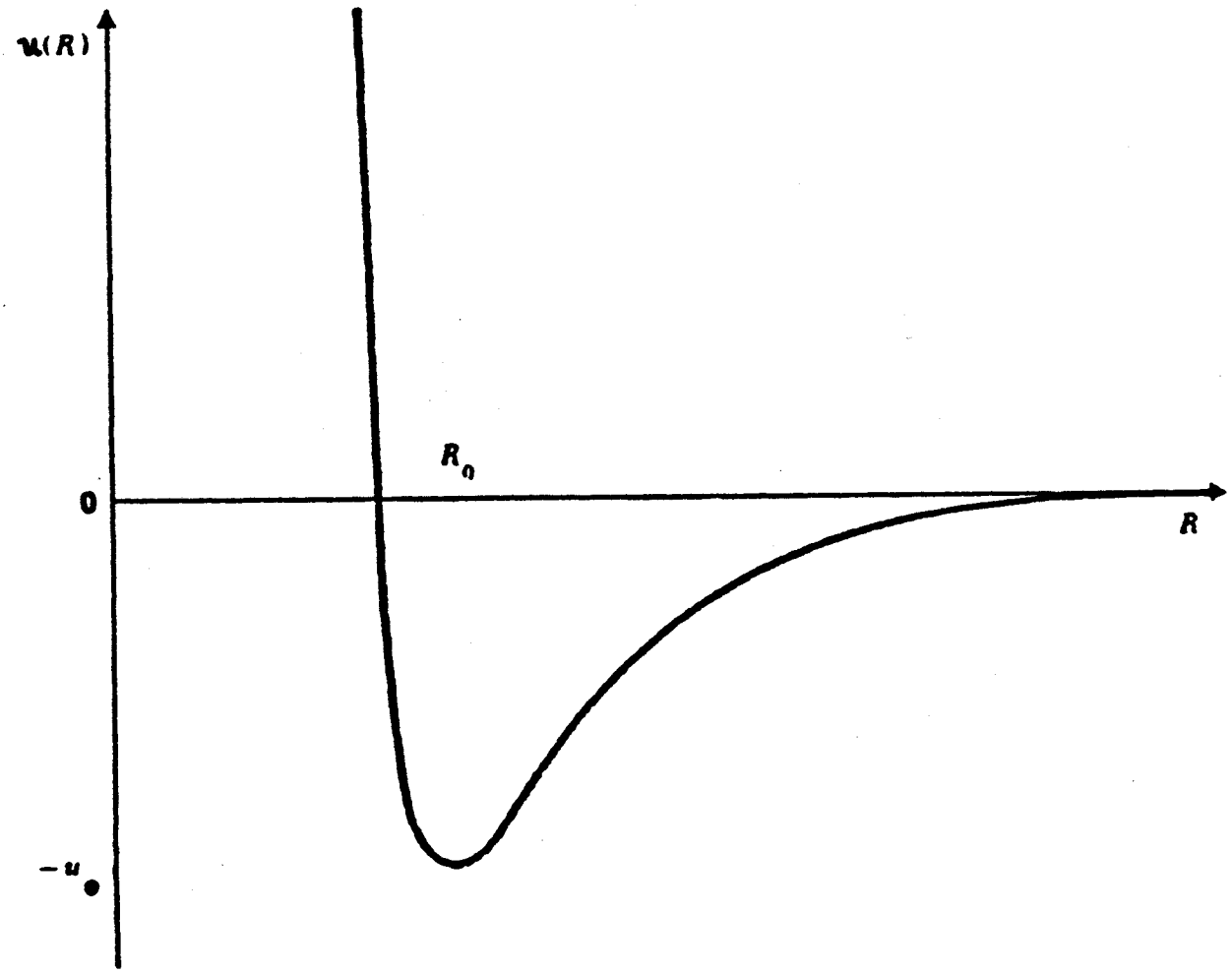

Figure 1. An energy density curve for a typical fluid. The coordinate R is the average separation between particles. At some equilibrium spacing R_o the energy per particle is a minimum.

$$K = 9 \frac{k}{\rho_0} .$$

Compressibility is not a well understood property of nuclear matter. Depending on how one parametrizes the interaction, the compressibility will vary. Empirically, the best value for K is about 200 MeV.[16] It will be a goal of our model to show how the results depend on what value is chosen for K. In physical terms if K is large the energy will rise sharply as the density is increased. Fluids with large K are relatively incompressible. A softer equation of state, small K, corresponds to a more compressible fluid. Three problems which will be of particular interest in modeling nuclear collisions will now be worked out.

The first question to consider is how the fluid will respond when a portion of it is disturbed from equilibrium by some outside force. The solution can be easily worked out, if the disturbance is small, by expanding the density and the velocity about their equilibrium values.[17] The equations of motion are:

$$\frac{\partial \rho}{\partial t} + \nabla \cdot (\rho \vec{u}) = 0 \qquad (1)$$

$$\rho \frac{\partial \vec{u}}{\partial t} + (\vec{u} \cdot \nabla) \rho \vec{u} + \nabla P = 0 \qquad (2)$$

In equilibrium, the fluid is at rest or in uniform motion. No fluid element has any relative velocity.

By small disturbances, it is meant that fluctuations in the density are small and the relative velocities remain small. Define the small function $\delta\rho(\vec{r},t)$ as

$$\rho(r,t) = \rho_0 + \delta\rho(\vec{r},t).$$

Substituting this into the equations of motion and keeping only first order terms, we find that small disturbances propagate through the fluid. The function $\delta\rho(\vec{r},t)$ obeys a wave equation and the velocity of the disturbance is closely related to the compressibility. The continuity equation becomes, to first order

$$\frac{\partial}{\partial t}\,\delta\rho(\vec{r},t) + \rho_0\nabla\cdot\vec{u}(r,t) = 0. \tag{3}$$

Euler's equation becomes

$$\rho_0\,\frac{\partial}{\partial t}\,\vec{u}(\vec{r},t) + c_s^2\nabla\delta\rho(\vec{r},t) = 0 \tag{4}$$

c_s^2 is defined as the derivative of the pressure with respect to density, evaluated at equilibrium density. Taking the time derivative of Equation (3) and subtracting it from the divergence of Equation (4) gives

$$\nabla^2\delta\rho(\vec{r},t) - \frac{1}{c_s^2}\,\frac{\partial^2}{\partial t^2}\,\{\delta\rho(\vec{r},t)\} = 0.$$

This is the equation for a wave whose velocity is given as

$$c_s = \left(\frac{\partial P}{\partial \rho}\right)^{\frac{1}{2}}$$

In terms of the compressibility the sound velocity can be written as

$$c_s = \left(\frac{K}{9m\rho_0}\right)^{\frac{1}{2}}$$

If K = 200 then for nuclear matter the sound velocity would be about .16 c. If large stresses are applied to the system such that densities substantially lower than ρ_0 are reached then, as can be seen from Figure 1, it is possible that $\frac{\partial P}{\partial \rho}$ will become negative. The point in the equation of state where the sound velocity becomes zero can be interpreted physically as that point where the fluid becomes unstable and breaks up. This negative maximum of the stress is a measure of the tensile strength of the fluid.

The next example illustrates a fluid undergoing a more massive disturbance, similar to the kind that must be considered in a nuclear collision. Consider a one dimensional slab of fluid traveling to the right with velocity u_0 and colliding with a stationary wall at time t = 0.[18] For the sake of simplicity it is assumed that no energy is dissipated. Qualitatively, the situation can be described as follows. Upon impact, there will be an increase in the density in the region

close to the wall. This will cause a pressure which slows down the incoming fluid elements. As more fluid is forced to rest, the boundary between the region of high density and normal density, hereafter called the shock front, will move to the left. The important parameters to discover are: 1) how fast the shock front propagates, and 2) what is the density of the fluid in the compressed region. Again, the conservation laws contain the solution. The following picture illustrates the problem.

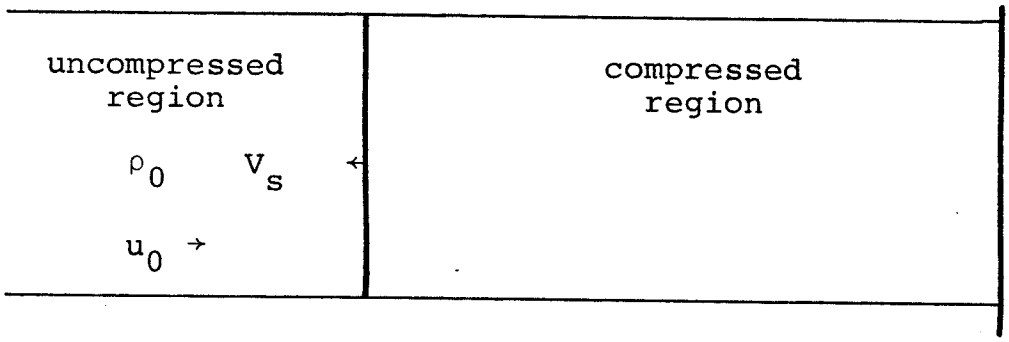

Consider what happens in a tube of unit area during a time interval Δt. During this time, the shock front will move a distance $V_s \Delta t$ to the left. A fluid element in the uncompressed region will move $u_0 \Delta t$ to the right. In order to conserve mass, it must be true that,

$$\rho V_s \Delta t = \rho_0 (u_0 + V_s) \Delta t.$$

It is also clear that the rate at which momentum is removed from the tube must be equal to the pressure in the compressed part.

$$\rho_0 u_0 (u_0 + V_s) = P(\rho)$$

These two equations are enough to determine the density of the compressed region and the velocity of the shock front, provided we also know the equation of state. This solution holds particular interest because it is also the solution to the problem of the collision of two slabs as seen in the center of mass frame. From these results the evolution of the system can be described quantitatively. At time t = 0 a shock-front begins to move from the wall to the left. The velocity of the front is given by

$$V_s = [P(\rho) - \rho_0 u_0^2]/\rho u_0$$

The kinetic energy of motion goes into increasing the density. This provides a pressure which brings the moving matter to rest. The density in the compressed region is given as the solution to the implicit equation

$$P(\rho) - \rho u_0/(\rho - \rho_0) = 0.$$

The shock front travels until it reaches the surface at the left where it is reflected back to the right. During this second stage fluid is ejected out of the compressed zone to the left with velocity u_0, and if there are no cohesive forces between the fluid and the wall it will leave having undergone an elastic bounce.

If the length of the slab is L, the time at which the slab leaves the wall is $t = 2L/V_s$.

There is one more idealized problem that must be solved before a complete description of the slab collision can be put together. This is the wave function of suddenly released compressed matter. Imagine a semi-infinite slab of matter in equilibrium and at rest. Suddenly, the right hand side is pulled away with velocity u_0.

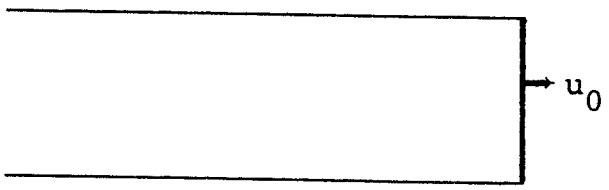

Because of the stress, a rarefied region will develop.[19] How low the density drops and how the rest of the fluid responds are the questions that must be answered. Because there are no characteristic lengths, it can be argued on dimensional grounds that the density and velocity can be written as functions of a new variable $\zeta = x/t$. A different argument for this goes as follows. From the theory of first order differential equations, it is known that a boundary condition and a first order differential equation are enough to uniquely specify a solution for all values of the independent variable. If the velocity and the density are known for some value

of ζ and it is also known how they change with respect to a change in ζ, then a solution exists for all ζ. Since the right hand edge is moving at $v = u_0$, ζ will always be u_0 at this edge. The boundary condition is

$$v(\zeta = u_o) = u_0.$$

At a point far enough away the density will be ρ_0,

$$\rho(\zeta = \infty) = \rho_0.$$

Using the relation $\frac{\partial}{\partial t} = -\zeta\frac{\partial}{\partial x}$ the continuity equation can be rewritten

$$(v - \zeta)\ \frac{\partial \rho}{\partial \zeta} + \rho\frac{\partial v}{\partial \zeta} = 0. \tag{5}$$

Similarly, Euler's equation becomes

$$\rho(v - \zeta)\ \frac{\partial v}{\partial \zeta} + c_s^2\ \frac{\partial \rho}{\partial \zeta} = 0. \tag{6}$$

These are two coupled first order equations for $\rho(\zeta)$ and $v(\zeta)$. Thus ρ and v are specified for all values of ζ. Dividing Equation (5) by Equation (6) gives a relation between the sound velocity, the fluid velocity, and ζ.

$$v - \zeta = c_s$$

Putting this back into Equation (5) gives

$$dv = \frac{c_s(\rho)}{\rho}\, d\rho .$$

Integrating across the rarefaction from $v = 0$ to $v = u_0$ tells how low the density will be at the edge.

$$u_0 = \int_{\rho_0}^{\rho_f} \frac{c_s(\rho)}{\rho}\, d\rho \qquad (7)$$

Another important number that is more easily obtained is how fast the edge can be pulled away before the fluid breaks up. Setting the upper limit in the integral (7) at ρ_c gives the upper limit on u_0. If the edge is pulled away faster than this critical velocity the density will become discontinuous.

With this result the slab collision can be understood. After contact a compression wave propagates in both directions outward from the point of contact. When the compression wave reaches the outer edge it is reflected back toward the center. When the two decompression fronts meet back at the center a rarefaction will develop. If visualized in a frame moving with one of the slabs it will appear as if the edge is suddently pulled away. The solution given above tells how low the density drops during the rarefaction.

CHAPTER IV

ONE-DIMENSIONAL MODEL

In order to describe the dynamics of nuclear matter, it is crucial to have a realistic equation of state. There are two properties of nuclei that must be reflected in this equation of state. These are the equilibrium density and the binding energy. Based on experiments that measure the size and the mass of nuclei, these values are taken as .16 nucleons/fm^3 and 16 MeV/nucleon respectively. Unfortunately there is no good theory from which an equation of state can be derived.[41] The best one can do at this stage is to write down a functional form. If the nucleus were a non-interacting Fermi gas then the energy per nucleon would be just the average value of the single particle kinetic energy,[20]

$$E/A = \left\langle \frac{p^2}{2m} \right\rangle .$$

If the particles also interact by a short range repulsive potential, then there is a contribution to the energy proportional to the density, assuming that the Fermi gas approximation is still valid. Finally, to

account for the saturation of nuclear matter we can add a density or velocity-dependent potential, depending on which model is used.[21,22,23] This gives a contribution to the energy that varies as $\rho^{\sigma+1}$, where σ may range between 1/3 and 5/3. This particular parametrization was suggested by Zamick[24] and it is the one we will use

$$E/A = \left\langle \frac{P^2}{2m} \right\rangle + A(\rho/\rho_0) + B(\rho/\rho_0)^{\sigma+1}.$$

Here ρ_0 is the equilibrium density. For a given value of σ the two constants A and B are fixed by knowing the binding energy and the saturation density. By considering different values of σ we are, in effect, allowing the compressibility to change. If we make the Thomas-Fermi approximation and assume that the particles always occupy a sphere of minimum radius in momentum space, then we can write the compressibility as a function of σ.[24]

$$K = [\left\langle \frac{P^2}{2m} \right\rangle + 9E_B + (3\left\langle \frac{P^2}{2m} \right\rangle + 9E_B)]$$

E_B = binding energy

We must now specify the stress tensor. There are two distinct limits that can be placed on the form of P_{ij}. In the simplest approximation we can say that P_{ij} is isotropic.

$$P_{ij} = \delta_{ij} P(\rho)$$

This is the approximation that is usually made for ordinary fluids. The stress tensor is also isotropic in the Thomas-Fermi model.[25] Physically this means that collisions between the nuclei are frequent enough so that a compression along one direction is followed by an increase in pressure along all directions within a time that is short compared to the time scale of the nuclear collision. In this limit the single particle kinetic energy can be written as

$$\left\langle \frac{P^2}{2m} \right\rangle = \frac{3}{5} \varepsilon_F (\rho/\rho_0)^{2/3}.$$

ε_F is the Fermi energy at equilibrium density. The pressure, which is now a scalar function of density, is given as

$$P = \rho^2 \frac{\partial}{\partial \rho} (E/A) = \rho_0 \left[\frac{2}{5} \varepsilon_F (\rho/\rho_0) 5/3 + A(\rho/\rho_0)\right.$$

$$\left. + B(\sigma + 1)(\rho/\rho_0)^{\sigma+2}\right].$$

On the other hand, if the collision rate is low and there is no mechanism by which momentum can be transferred from one direction to another, then the different directions will remain uncoupled. This leads to the kind of stress tensor that is used to describe an elastic material. A compression along the z direction

causes a pressure along the z direction only. This will change the dependence of the kinetic energy on the density.

$$\left\langle \frac{p^2}{2m} \right\rangle = \left\langle \frac{p_x^2}{2m} + \frac{p_y^2}{2m} \right\rangle + \left\langle \frac{p_z^2}{2m} \right\rangle = \frac{2}{5}\,\varepsilon_F + \frac{1}{5}\,\varepsilon_F\,(\rho/\rho_0)^2$$

We will now construct a model for the collision of two slabs of nuclear matter. A Langrangian method is used to numerically integrate the fluid dynamic equations.[26] Individual fluid elements are tagged and may be thought of as particles. Imagine a string of particles whose equilibrium spacing is r_0. That is, if $r > r_0$ there is an attractive force which pulls them together. If $r < r_0$ there is a repulsive force which pushes them apart. At equilibrium the particle density is

$$\rho_0 = \frac{1}{r_0} .$$

If forces act which cause the particles to get closer together the density will increase. If these forces are conservative then the work done will cause an increase in the internal potential energy. Similarly, a decrease in density will also cause an increase in energy. The force on each element is obtained from the stress tensor.

$$F = \frac{1}{r_0}\{\frac{2}{5}\,\varepsilon_F(\frac{r_0}{r})^{\alpha} + A(\frac{r_0}{r}) + B(\sigma + 1)(\frac{r_0}{r})^{\sigma+2}\}$$

$$\alpha = 3 \text{ (elastic)}$$

$$\alpha = \frac{5}{3} \text{ (fluid)}$$

An equation of motion is written for each fluid element,

$$m\ddot{r}_i = F(r_i,r_{i+1}) + F(r_i,r_{i-1}) = F(r_i).$$

From the configuration of the system at time t the force is calculated. The new velocities are

$$v_i(t + \Delta t) = (F(x_i,t)/m)\Delta t + v_i(t)$$

The new positions are

$$x_i(t + \Delta t) = x_i(t) + v_i(t)\Delta t.$$

One of the more interesting results of this model is the energy at which the system breaks up. The most important parameter in determining this breakup energy is the tensile strength of nuclear matter. The critical density, along with several other important characteristics of the equation of state associated with the breakup threshold, are presented in Table 1. The critical density remains between about .64 ρ_0 - .68 ρ_0 for all of the cases considered. In the elastic model, however, more energy is required to achieve critical density.

Table 1. The important quantities related to the breakup threshold of nuclear matter. The different values of σ correspond to different compressibilities.

Equation of State σ =	Critical density ρ_c	Maximum pressure (MeV/fm^3)	$\frac{E}{A}(\rho_c) - \frac{E}{A}(\rho_o)$ (MeV)
1	.68	3.5	2.2
fluid			
$\frac{1}{3}$	.64	2.4	1.8
1	.68	5.2	3.5
elastic			
$\frac{1}{3}$	.64	4.2	3.2

Table 2. The critical velocity at which breakup occurs for the different equations of state. These are calculated using Equation III-7.

Equation of State σ =		Critical Velocity	Critical Energy (MeV)
fluid	1	.048	1.1
	$\frac{1}{3}$	.045	.94
elastic	1	.062	1.8
	$\frac{1}{3}$	.058	1.6

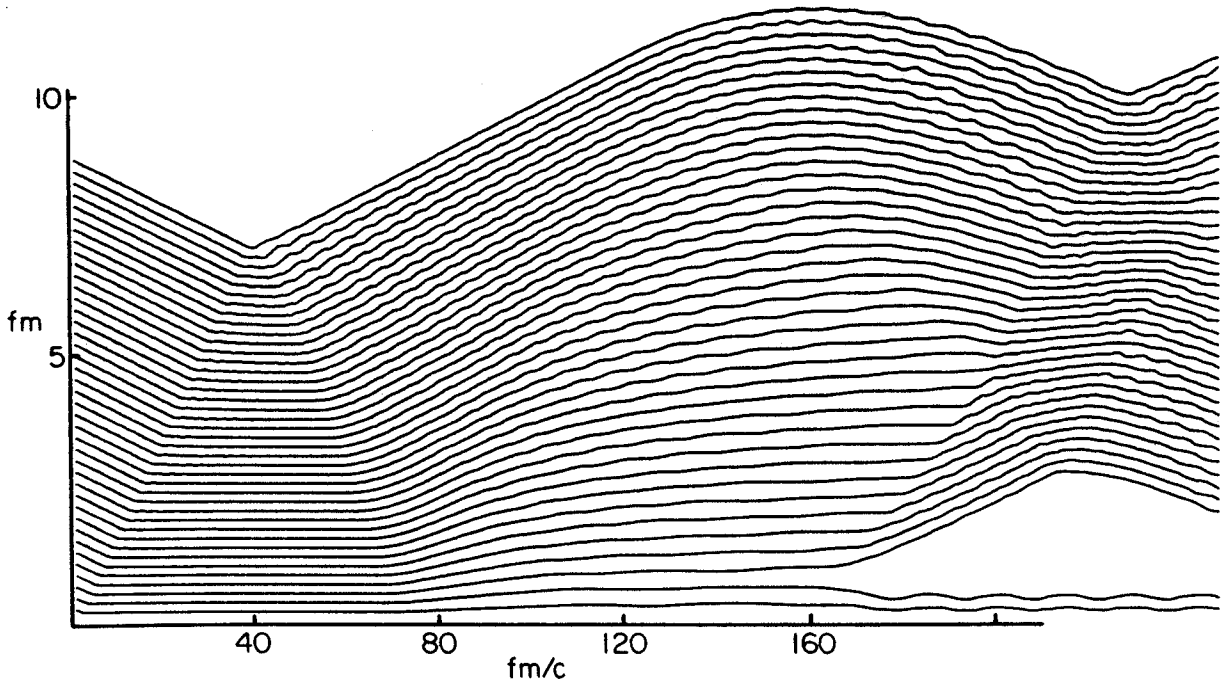

Figure 2. Slab collision at 1 MeV/A (c.m.). The position of mass elements as a function of time is shown for half of a symmetric collision of two slabs, each 9 fm. thick. The slabs just make contact at t = 0; the equation of state is the fluid model with $\sigma = 1/3$. Maximum compression occurs at 40 fm/c and the system snaps at $\cong$ 160 fm.

These numerical studies verify the behavior that was described in Section III.[27] The numerical values for the breakup energy and velocity are given in Table 2. Figure 2 shows a graphic representation of a slab collision. Each line represents the motion of a tagged fluid element. In this calculation, we used a time step $\Delta t = 1$ fm. The compression and rarefaction wavefronts are clearly visible. The first two stages of the collision are completely described in the analytical treatment given above. The third stage shows some interesting features that require further discussion. First of all, the energy required for breakup is somewhat higher than the predicted value.[27] This happens because the forces have a finite range. Even though the density may have fallen below the critical value, there are still forces between the fluid elements. Furthermore, the development of an instability requires a finite amount of time. The time required will depend on the energy. If the energy is more than 50 percent above threshold then the system will break up quickly. On the other hand, if the energy is only slightly above threshold, the rarefaction will have propagated a large distance during the time it takes for the instability to develop. During this stretching it may happen that enough momentum is removed from the center of mass

motion so that the system does not come apart. Because of the stretching, the energy associated with the relative motion of the slabs after separation can be considerably less than the incident energy. This particular feature will come up again when we discuss energy loss in deeply inelastic heavy ion collisions.

CHAPTER V

DESCRIPTION OF THE MODEL AND COMPUTATIONAL TECHNIQUE

We want to use the results of the one-dimensional calculation to create a more general model of the collision of two nuclei in three dimensions. The computational approach, however, will be quite different. Recall the technique in the slab sollision was to tag many fluid elements and then follow the motion of each as the system evolved. This works if the system is simple enough, but gets very complicated for a three dimensional calculation. What can be done instead is to parametrize the motion. This will reduce the number of degrees of freedom, while still keeping a valid description, provided the parametrization is chosen properly. For example, knowing the form of the solution, the one-dimensional slab collision can be described with just one variable. This is the location of the shock front.

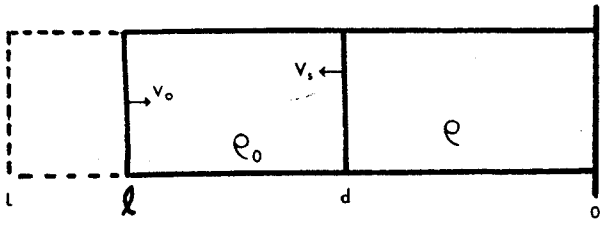

The continuity equation becomes

$$L\rho_0 = \rho_0(\ell - d) + \rho d,$$

where L is the initial length of the slab, ℓ is the length at time t, and d is the location of the shock front at time t. The fluid between ℓ and d moves to the right with uniform velocity v_0. Assuming the fluid to the right of the shock front in the compressed region to be at rest, then Euler's equation becomes, in the integral form,

$$\rho_0 v_0(v_0 + V_s) = P(\rho).$$

It is convenient to use the coordinate of the center of mass x_{cm}.

$$x_{cm} = \int_0^{\ell} x\rho(x)dx = [\tfrac{1}{2}\rho d^2 + \tfrac{1}{2}\rho_0(\ell^2 - d^2)]/L\rho_0$$

The velocity of the center of mass is

$$Mv_{cm} = \rho_0[\ell v_0 + \tfrac{1}{2}\ell V_s - \tfrac{1}{2}LV_s - \tfrac{1}{2}dv_0].$$

The acceleration of the center of mass is

$$Ma_{cm} = M\frac{\partial}{\partial t}v_{cm}(d) = \rho_0 v_0(v_0 + V_s) = P(\rho). \qquad (1)$$

To solve the dynamics, a best guess is made for d. The new configuration is specified and the acceleration of

the center of mass is calculated. A variation is then done on d and again the acceleration is calculated. The first derivative is defined as

$$\frac{\partial a_{cm}}{\partial d} = \frac{a_{cm}(d_0 + \delta d) - a_{cm}(d_0)}{\delta d}.$$

On a small enough time scale, the force and the acceleration will change slowly enough so that the force from the previous time step can be used to calculate the acceleration. Using a first order Taylor series expansion the equation for δd is

$$P(\rho) = a_{cm}(d_0) + \frac{\partial a_{cm}}{\partial d}\,\delta d.$$

In the next step set $d = d + \delta d$ and again calculate $a_{cm}(d)$. If the quantity $Ma_{cm}(d) - P(\rho)$ has a magnitude less than some small number, then this time step is complete. If not, then d is put forward as the best guess and the whole algorithm is reiterated.

For the three-dimensional model we will follow this same general procedure. The system will be parametrized in such a way as to keep the number of degrees of freedom small while still retaining the features that are important to the theory. The features that are to be included are the following. 1) The idea that nuclear matter can be represented by an equation of

state and that during the collision a shock wave will form. The velocity of the shock front and the density that is maintained in the compressed region will depend on this equation of state. 2) Because the particles on the surface are less bound, there is an energy proportional to the surface area. This causes a surface tension which tends to minimize the surface area. 3) The charges on each nucleus give rise to a Coulomb repulsion.

The kinds of information to be supplied from the model are the general features that can be observed experimentally. The angular distribution, which in a classical model comes from a deflection function, will be studied. At lower energies fusion cross-sections will be calculated. Energy loss and angular momentum transfer are also topics that will be explored. All of these results will depend on the equation of state. The nature of this dependence will be of primary interest.

The collision of the two nuclei is parametrized in the following way. The shape of each nucleus is assumed to remain spherical. In fact, because of the compression there will probably be some distortion of the shape in the region of higher density. This may be important in dissipating energy. In this model we neglect this distortion. Take the reaction plane to be the $z = 0$ plane. The coordinates (x,y) will specify the location

of the center of the sphere. These will be two of the parameters used. The shock wave is taken to be a plane wave which travels along the line connecting the centers of the two spheres. The location of the shock front will be the third parameter. The following figure illustrates a head-on collision at some instant in time.

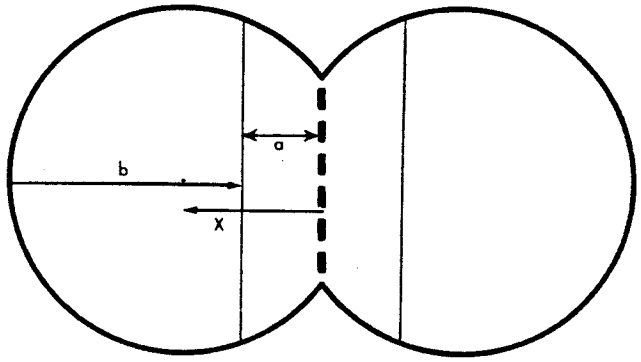

Assuming the compressed region to be at uniform density, the continuity equation becomes

$$\rho_0 \frac{4}{3} \pi R^3 = \int \rho dV + \int \rho_0 dV'$$

The velocity field in the compressed region is taken to be zero while the uncompressed region moves with a uniform velocity v. Euler's equation will give the shock velocity at the point of impact.

$$\rho_0 v(v + V_s) = P(\rho)$$

V_s is then assumed to remain constant during the collision. For collisions at a non-zero impact parameter

the situation is similar if viewed from a rotating frame.

As in the one-dimensional case the forces arising from the pressure, Coulomb repulsion, and surface tension are taken to act on the center of mass coordinates. The Coulomb repulsion is taken as the force between two point charges located at the center of mass of each nucleus. In calculating the force from the surface tension we have used the following picture.

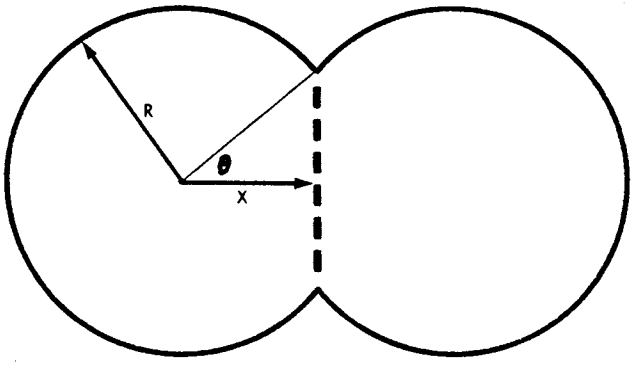

The surface energy is taken from the liquid drop model[28] to be 1 MeV/fm^2. If the separation between centers changes then the surface area will change. The change in area with respect to a change in separation is proportional to the force. The area can be written as a function of x,

$$\text{Area} = 2\pi R^2 \int_{-1}^{x/R} d(\cos\theta) = 2\pi R^2 \left(\frac{x}{R} + 1\right).$$

The force is given as

$$\text{Force} = \sigma\frac{\partial}{\partial x}\,(\text{Area}) = 2\pi R\sigma.$$

σ is the surface energy and R is the radius of the nucleus. Using this expression for the surface force will underestimate its strength during the initial stage of the collision since a neck region will be forming. During the breakup stage when the neck is stretching it will overestimate the surface force. However, since the shape of the neck has not been parametrized this seems to be the only reasonable assumption. The compressed region will exert a pressure at the boundary between the two nuclei. This has two components. There is a radial force equal to the pressure times the area of the boundary. The force is given by

$$F_r = P(\rho)\pi(R^2 - x^2),$$

where 2x is the distance between the centers of the nuclei. This will be a repulsive force acting in the same direction as the coulomb force. The surface force is also radially directed but it is attractive.

The second component of the pressure is a tangential force which comes from the flux of particles, with tangential momentum, across the boundary. This acts like a friction force removing energy from the collective

motion. This energy goes into other degrees of freedom. The momentum flux is calculated by integrating over the phase space distribution function.

$$T_{||} = \int p_{||} v_{\perp} f(r,p) d^3p$$

This integral can be done explicitly using the Fermi gas model. In momentum space the distribution can be drawn as two displaced spheres.

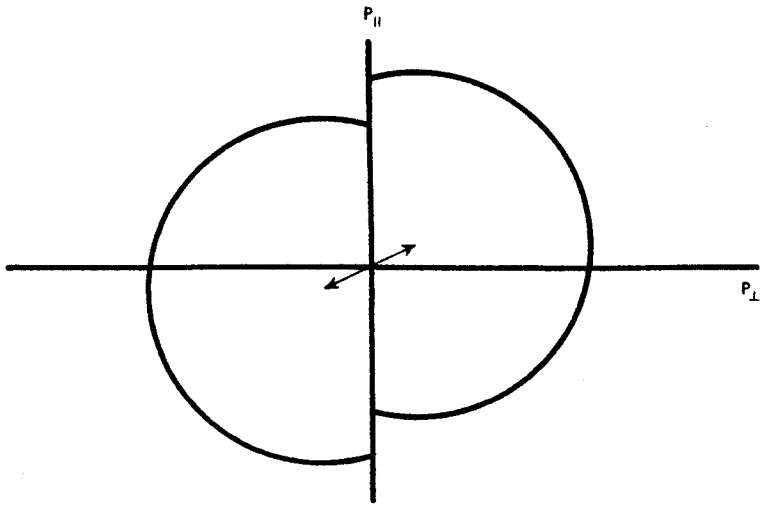

This leads to the following expression for $T_{||}$

$$T_{||} = 3\rho\varepsilon_f V[1 - \alpha^2)(1 + \alpha)^3/3 + \frac{2}{3}\alpha(1 + \alpha)^3$$

$$- \frac{1}{4}(1 + \alpha)^4],$$

where $\alpha = \frac{v}{v_F}$, and $\nu = \frac{v_{||}}{v_F}$. v_F is the Fermi velocity. In the limit of small velocities this reduces to the approximate expression

$$T_{||} \cong 3\rho\varepsilon_F \nu(\tfrac{1}{4}).$$

The force itself is given by

$$F_t = T_{||} (R^2 - x^2).$$

F_t is taken to act on the center-of-mass coordinate of each nucleus, changing the tangential component of its momentum. The tangential force also causes some of the orbital angular momentum to be transferred to intrinsic angular momentum of the nuclei.

The equations of motion for the center of mass coordinates are

$$a^x_{cm}(t) = \frac{\partial}{\partial t} \{\frac{x_{cm}(x,y,d;t+\Delta t) - x_{cm}(x,y,d;t)}{\Delta t}\} = \frac{F_x}{M}$$

$$a^y_{cm}(t) = \frac{\partial}{\partial t} \{\frac{y_{cm}(x,y,d;t+\Delta t) - y_{cm}(x,y,d;t)}{\Delta t}\} = \frac{F_x}{M}$$

These are both implicit equations for the parameters x,y,d. The computational technique used is just a generalization of the one dimensional case cited earlier. Based on the previous history of the system, a best choice is made for the new configuration. A variation is then done on each parameter and the first derivatives are calculated. The small changes are calculated from a first order Taylor series expansion. This technique

seems to work very well. It converges rapidly onto the correct solution, and the errors can be easily specified. It is also quite stable and allows a coarse time step to be used. An interval of t = 1 fm/c was used in the calculation. This provided sufficient accuracy with a minimum of computer time. During the final stage, when the system is breaking up, the lower density causes a negative pressure which provides an attractive force. If the velocity is larger than the critical value obtained in the one-dimensional model, then the system will break up. The amount of stretching that takes place before separation is taken over directly from the one-dimensional model.

CHAPTER VI

APPLICATION OF THE COMPRESSIBLE FLUID MODEL TO ENERGY LOSS

In our model there are two mechanisms by which energy is lost from the relative motion. For energies well above the fusion barrier the primary cause of energy loss is the flux of tangential momentum across the boundary separating the two nuclei. This acts like a friction force, removing momentum at a rate proportional to the tangential velocity. The largest losses will occur when the impact parameter is around .5 R. For collisions at low energies, just above the fusion barrier, there can be a considerable amount of energy lost from the relative motion because of the finite distance the rarefaction travels before the nuclei break apart. In this case the energy goes into producing a rarefied region of nuclear matter in which each nucleon is bound by an energy less than 16 MeV. Both the frictional force and stretching are one-body processes. In Section IX we will also take into account the energy loss due to nucleon-nucleon collisions.

Experiments done at energies just above the Coulomb barrier show a large cross section for strongly damped

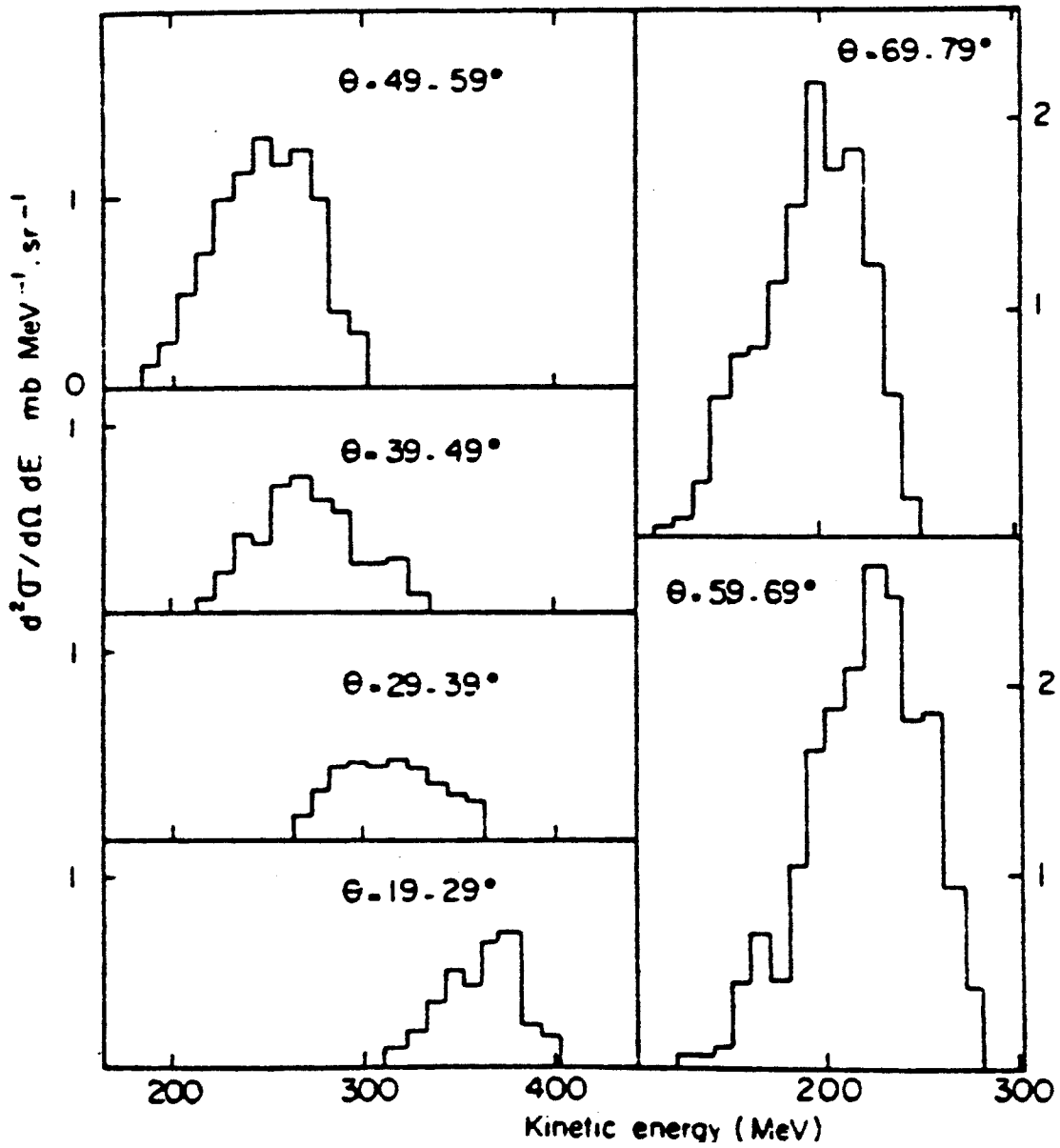

Figure 3. The energy distribution of the quasi-Kr products observed as a function of angle. The reaction is 525 MeV ^{84}Kr on a ^{208}Pb target.

collisions. Looking at the energy loss as a function of angle one finds, aside from the elastic peak, a broad energy distribution centered near the Coulomb energy. Figure 3 shows a typical distribution as seen in the lab frame.[29] Energies below the Coulomb barrier are commonly observed which indicates that there is some deformation of the system before separation.

The following figures illustrate the results of the compressible fluid model as it applies to energy damping. The two fragments are assumed to follow Coulomb trajectories after scission. The kinetic energies referred to include this Coulomb energy. Figure 4 shows how the energy loss depends on the compressibility. The ratio of the scattered particle's kinetic energy to the incident energy is plotted as a function of angle for two different equations of state. The two cases considered correspond to compressibilities of 200 MeV and 500 MeV. These represent the extreme values of K. The nuclear system used in this example is $^{84}Kr + ^{84}Kr$ at an incident energy of 4 MeV/nucleon in the center of mass frame. The energy of the outgoing fragment ranges from E_{inc}, for a nearly grazing collision to a value slightly below the Coulomb energy of two touching spheres. The energy loss is less for the softer equation of state (K = 200). To understand this result recall

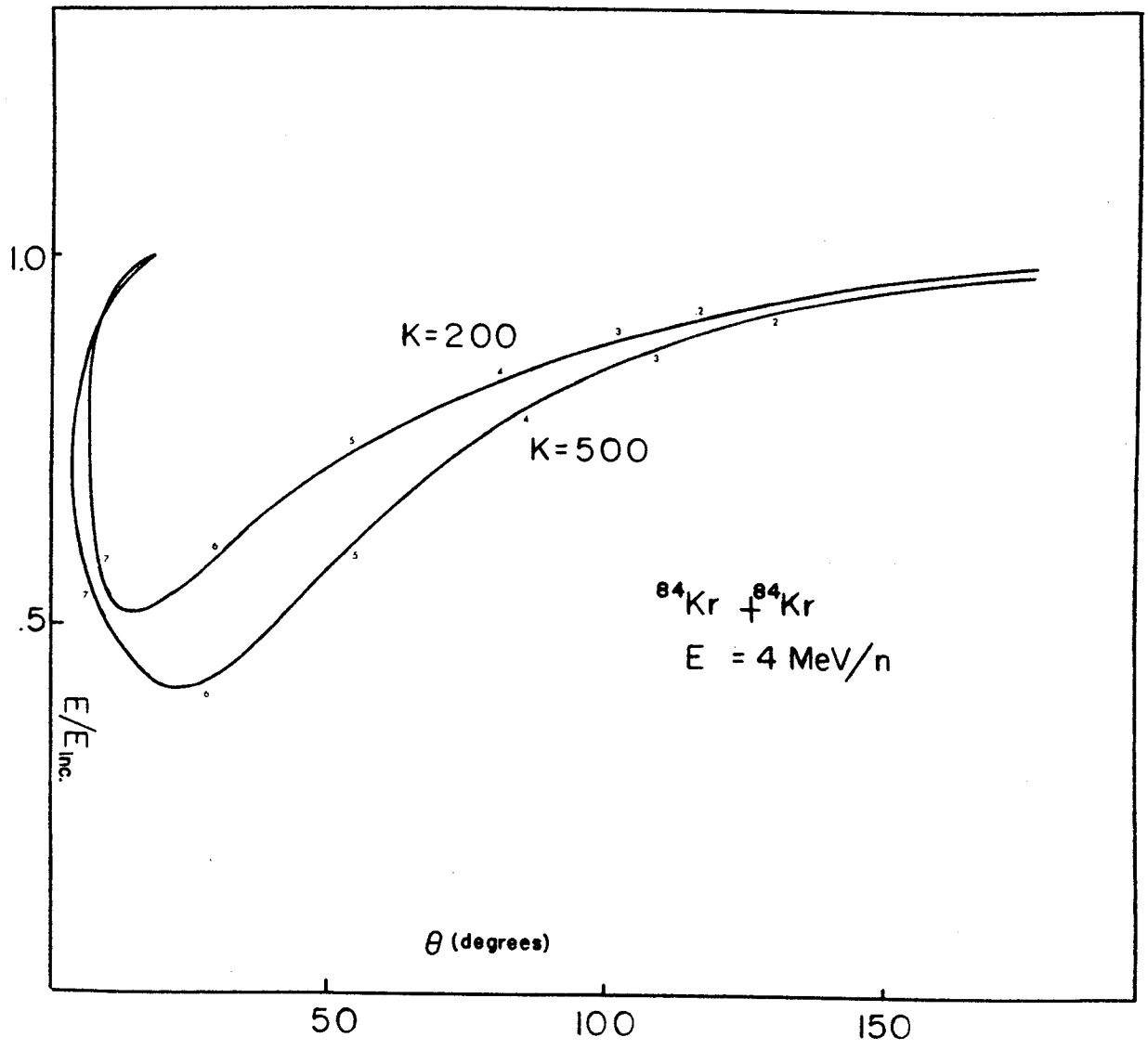

Figure 4. The energy loss depends somewhat on the equation of state. Here energy loss is plotted as a function of angle. E/E_{inc} is the fraction of energy left in the scattered nucleus.

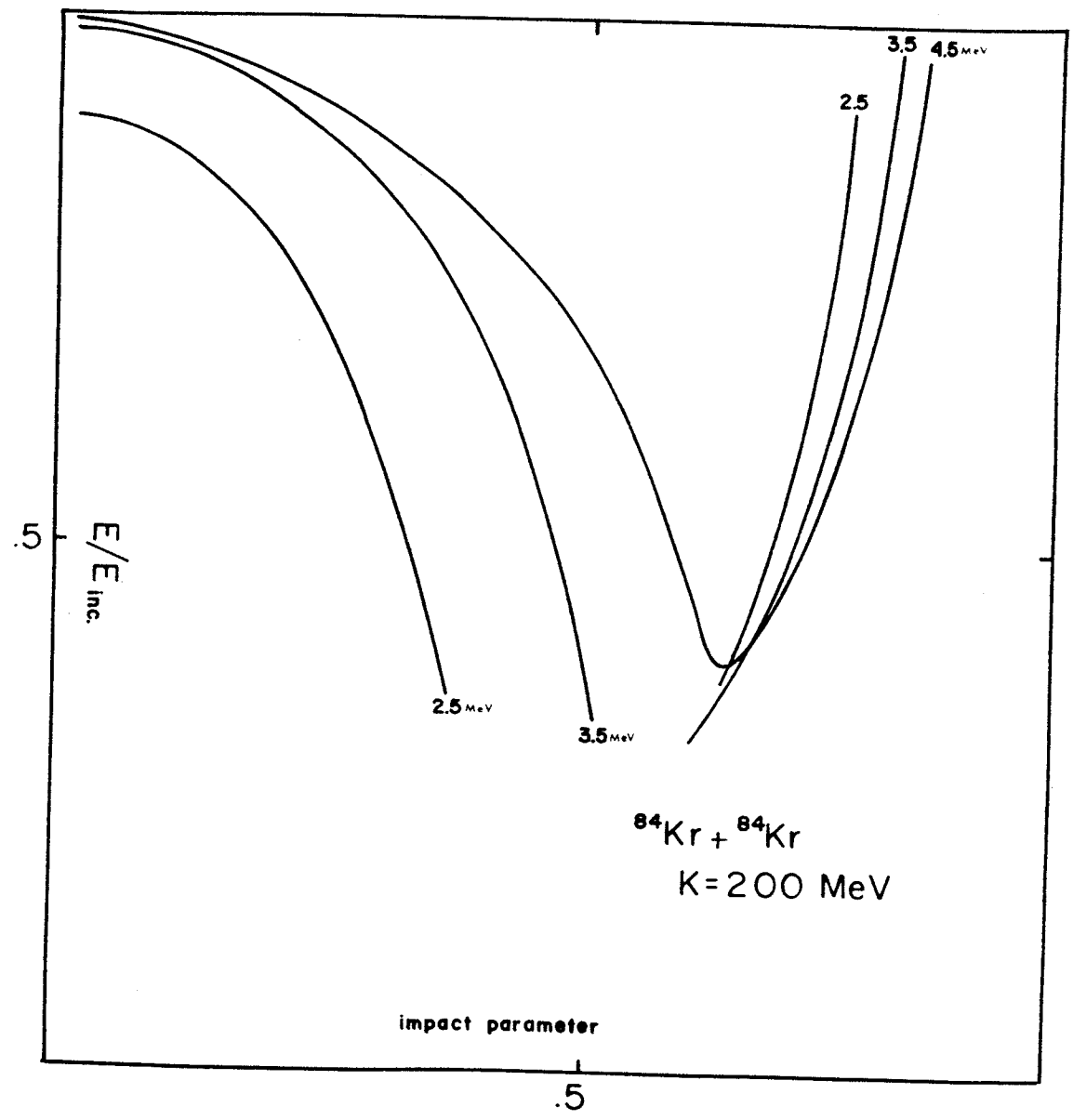

Figure 5. The fraction of energy left as a function of impact parameter at center of mass energies of 2.5, 3.5, and 4.5 MeV/A.

from Table 1 that the critical velocity, which is a measure of the strength of a fluid, is lower for a softer equation of state. This lower critical velocity means that the system will not stretch as much before snapping, leaving more energy in the relative degree of freedom.

Figure 5 shows the fraction of energy left as a function of impact parameter. For an incident angular momentum greater than the grazing value there will be no energy loss in this model. In fact, there may be some energy loss due to Coulomb excitations. This mechanism has not been considered here. As the angular momentum decreases to slightly below the grazing value there is still very little overlap between the colliding nuclei. The length of time during which contact is maintained is also short. Based on this one would expect the energy loss to be small. As the impact parameter becomes even smaller the energy loss increases sharply until it reaches a maximum value at about b = .5. In this range the contact between the two nuclei is solid and there is substantial energy loss due to the flux of tangential momentum. These results up to this point show very little energy dependence other than the obvious dependence of L_g on E_{inc}. For small impact parameters the energy loss does depend somewhat on the incident energy. High energy collisions are quick and

the nuclei have a tendency to bounce off from each other with very little dissipation of energy. As the energy decreases the nuclei begin to appear sticky to each other. The analogy to silly putty, which has been used to describe heavy ion collisions, is appropriate here. In Figure 6 we present the results in the form of a Wilczynski plot.[45] This is the kind of information one would obtain from experiment. At the more forward angles there may be two or three distinct energy peaks. This happens because two or three very different trajectories may finally scatter into the same angle. The largest energy losses are observed at quite forward angles. The cause of this is the onset of nuclear orbiting which will be discussed further at a later point. Again at the large angles which correspond to small impact parameters there is some energy dependence. For low energy collisions just above the Coulomb barrier there will, of course, be no back scattering because of fusion. The small numbers on each curve give the impact parameter that corresponds to the angle. This provides a relative measure of the cross sections. This particular plot is for $^{40}Ca + ^{40}Ca$ at energies over the range of 2 to 5 MeV/nucleon. Using the results of energy loss as a function of impact parameter it is possible to derive another kind of cross section

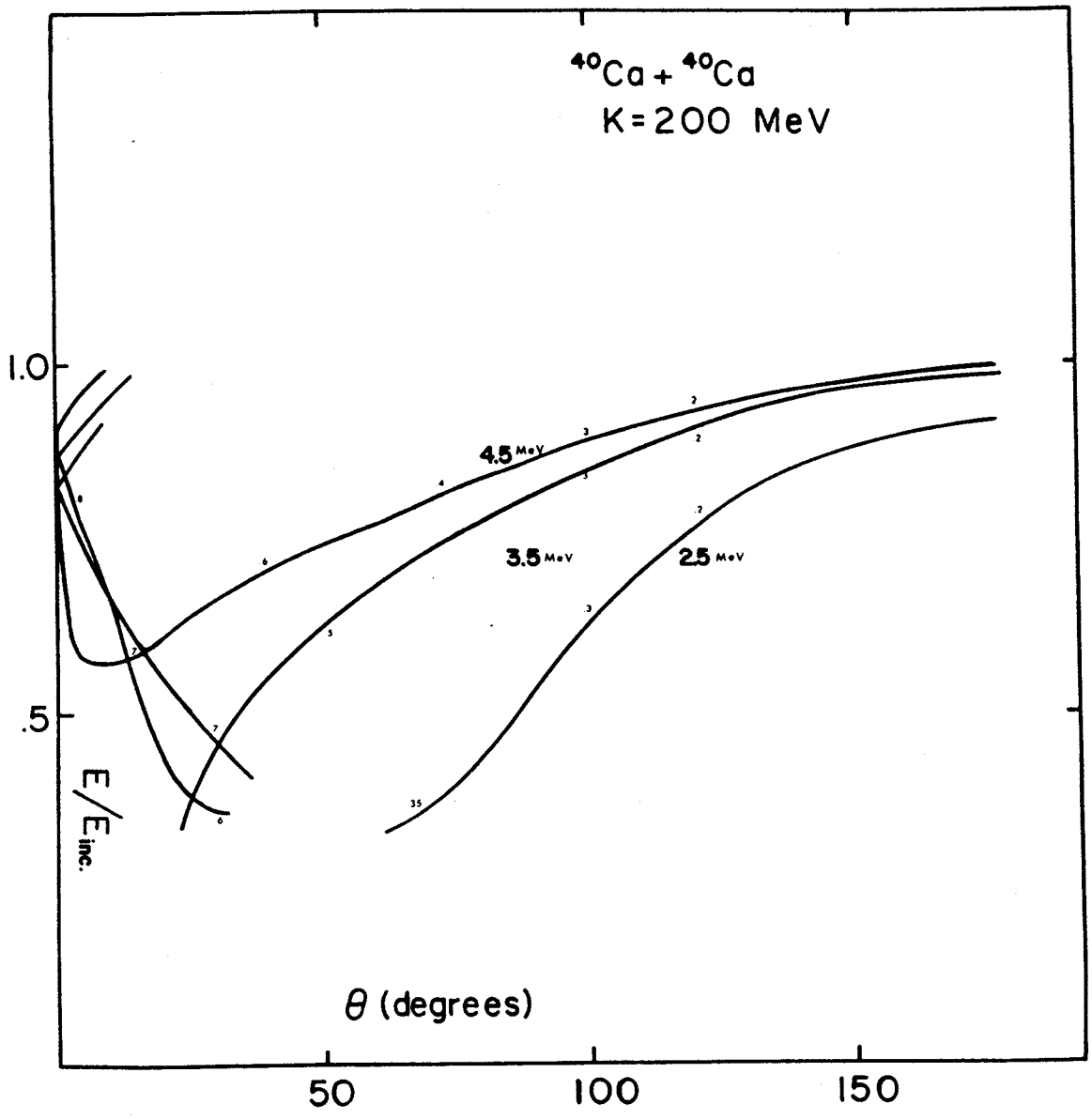

Figure 6. The fraction of energy left in the outgoing fragment versus the scattering angle. The small numbers indicate the impact parameter.

$$\frac{d\sigma}{dE} = 2\pi b \frac{db}{dE}$$

Physically this corresponds to plotting the number of counts in the energy range dE as a function of energy, integrated over all angles. Figure 7 shows $\frac{d\sigma}{dE}$ versus E for the reaction $^{84}Kr + ^{84}Kr$ at 5 MeV/nucleon. The fairly sharp peak comes from the peak in energy loss at $b \cong .6$ R.

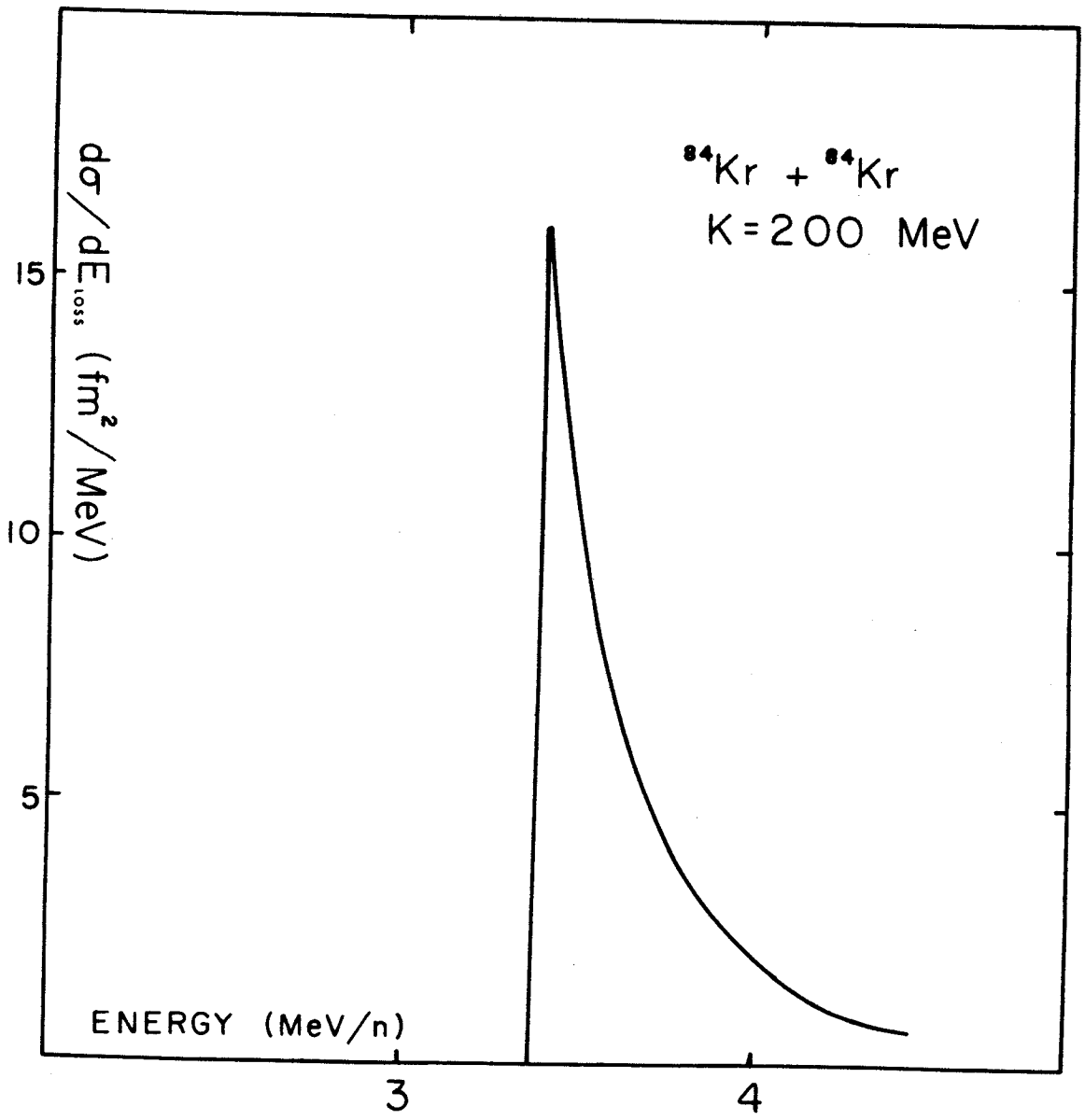

Figure 7. Energy distribution of the outgoing nuclei integrated over all angles.

CHAPTER VII

APPLICATION OF MODEL TO FUSION

When two heavy ions collide with energy in the range of 1-6 MeV/nucleon, and if the angular momentum is not too large, then there is a good possibility that the two nuclei will fuse together, forming a compound nuclear system. Cross sections for fusion have been measured on a variety of systems at energies up to about 5 MeV/nucleon. (Energies quoted will always refer to the center of mass coordinate system.) A detailed account of many fusion experiments has been compiled by Birkelund and co-workers.[30] From these experiments the general features of the fusion cross section can be described. At energies below the Coulomb barrier fusion is improbable. As the energy increases above the Colomb barrier, the cross section rises sharply. At about 4 MeV/nucleon it reaches a maximum. As the energy is increased further the cross section starts to decline. Above 5 or 6 MeV/nucleon it is expected to continue this decline, but there is no data available to verify this. The maximum cross section is typically one barn.

Before presenting the results of our calculation it will be useful to discuss briefly how fusion occurs in this compressible fluid model. For energies below the Coulomb barrier no contact is made and the fusion cross section is predicted to vanish. At these energies the nuclei follow purely Coulomb trajectories. As the energy is increased the range of impact parameters over which contact occurs becomes larger. When contact is made the surface tension and the cohesiveness of nuclear matter favor fusion. As the energy is increased further contact is made with relative velocity. In this case a region of higher density is formed. Some of the relative kinetic energy will go into increasing the density and the rest will be dissipated by the frictional force, exciting internal degrees of freedom. The compound system will go through compression, decompression, and rarefaction. The relative velocity of the two nuclei along with the impact parameter will determine the intensity of the oscillations, which in turn will determine whether the system remains fused or breaks apart during the rarefaction. Depending somewhat on the equation of state, nuclear matter has enough cohesiveness to hold the system together if the rarefaction is not too strong. At low impact parameters a larger portion of the kinetic energy goes into the compression. This

energy, stored in the first stage of the collision, is then available in the second stage to accelerate the two nuclei apart. This phenomena suggests that the two nuclei are bouncing off from each other. The critical energy for breakup is lower for the smaller impact parameter. The critical energy will increase as the impact parameter increases because of the increasingly larger amounts of energy dissipated by the tangential friction. This has the effect of damping the oscillations and reducing the intensity of the rarefaction. As the collisions become more grazing the overlap becomes less and the centrifugal force will set the upper limit on the range of impact parameters for which fusion occurs at a given energy. All these arguments can be incorporated in a very simple model if friction is neglected. The nuclei follow Coulomb trajectories up to the point of contact. At this point, if the radial velocity is less than some critical value, which will depend on the equation of state, and if the centrifugal force plus the Coulomb repulsion is less than the surface tension, then the two nuclei will remain fused. If these conditions are not satisfied the system will break up and a scattering event will take place. This simple model exhibits the features of the more detailed model regarding the fusion cross section. It allows one to

calculate directly the fusion cross section for any nuclear system. The effect of including friction will be to increase the cross section at the higher energies.

The results of the full calculation have been tabulated for a wide range of nuclear systems, from ^{40}Ca to ^{134}Xe. Figure 8 shows the range of impact parameters for which fusion occurs as a function of energy. One can clearly see the bouncing effect at low impact parameters. At the highest energies, fusion takes place only at b $\cong$ .5 R. It is in this range that the largest amount of energy is lost. The top smooth curve represents a grazing collision. For impact parameters above this line, the scattering is pure Coulomb. Note also that at higher energies the maximum impact parameter decreases as the energy increases. This indicates the increasing importance of the centrifugal force. From Figure 8 it is clear that larger systems are more likely to break apart after having made contact. This is due largely to the Coulomb repulsion. Figure 9 shows the total cross section as a function of energy. The peak occurs at between 2 and 3 MeV/nucleon. The fraction of the total cross section available for fusion decreases as the number of nucleons increases. Figure 10 shows the dependence of the fusion cross section on the equation of state. The reaction

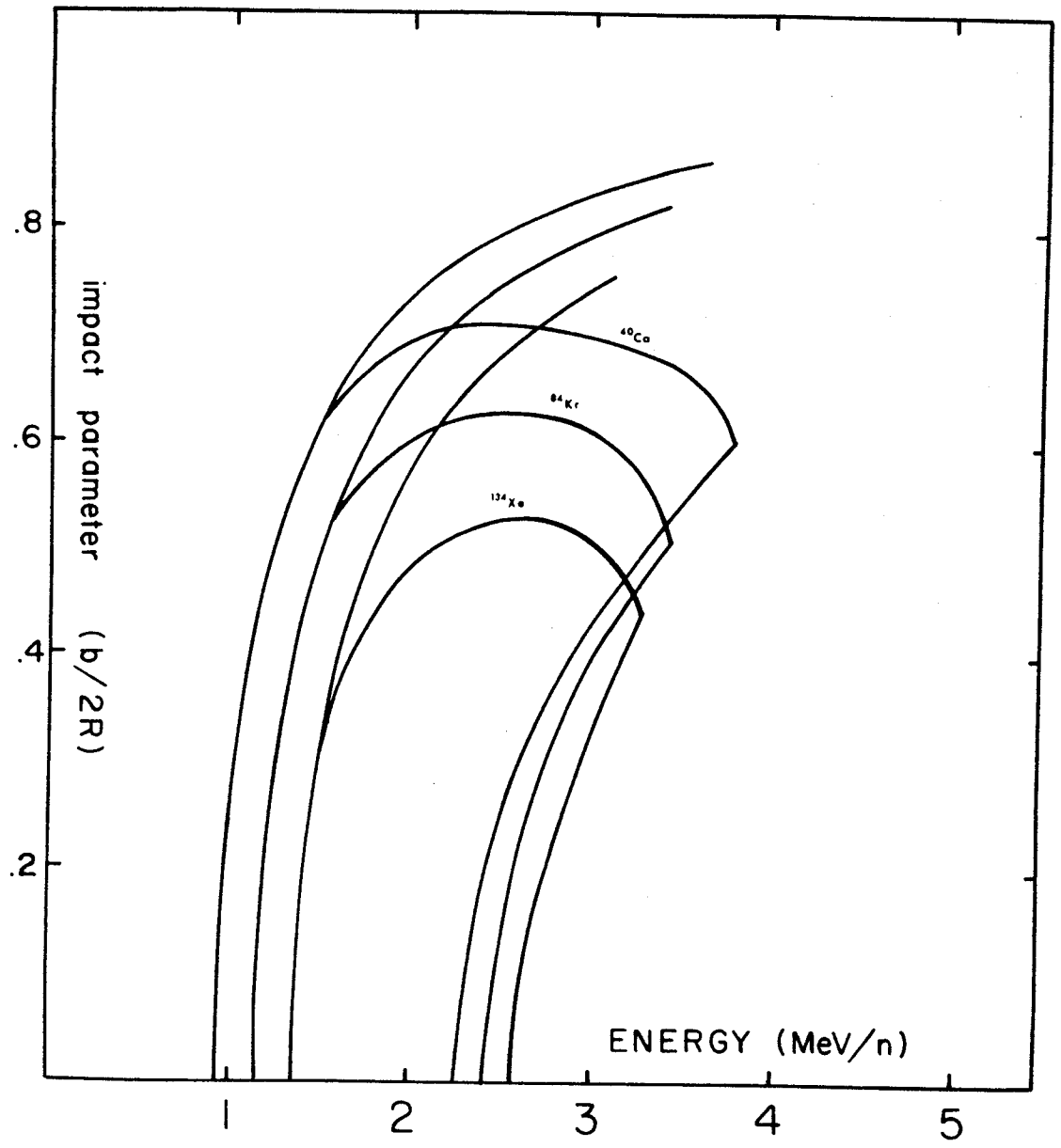

Figure 8. The energy-impact parameter area in which fusion occurs. The extended curve represents a grazing trajectory. The compressibility is K = 500 MeV.

is $^{40}Ca + ^{40}Ca$ at K = 200 MeV. The effect is not large and seems to have no effect on the low energy collisions. As the energy increases the cross section falls off more rapidly for small K. This happens because the critical velocity increases as the compressibility increases. In effect the softer fluid is less sticky and unable to hold together under large tear away forces.

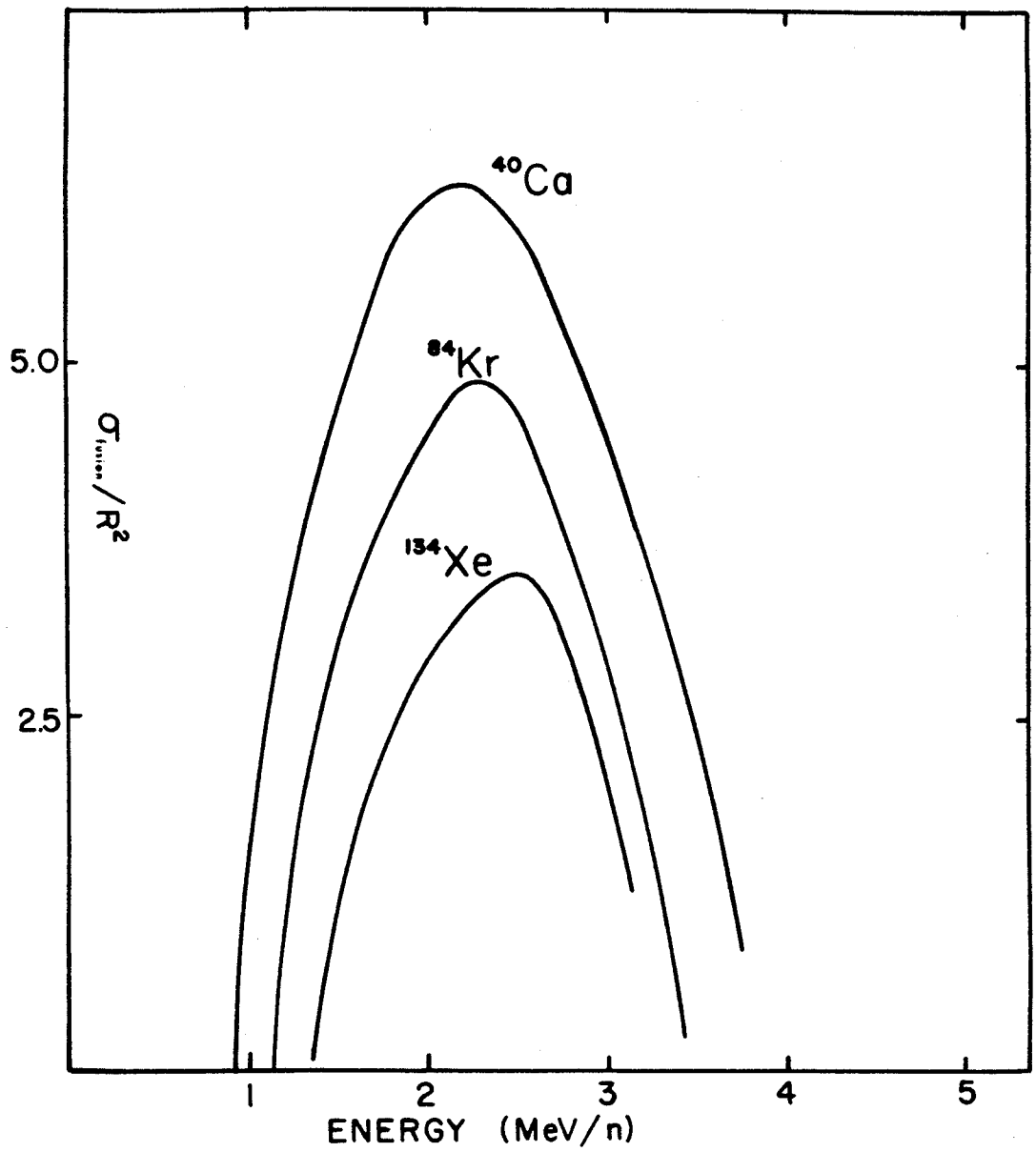

Figure 9. Energy dependence of the fusion cross section for three different systems, ^{40}Ca(^{40}Ca,^{80}Zr), etc.

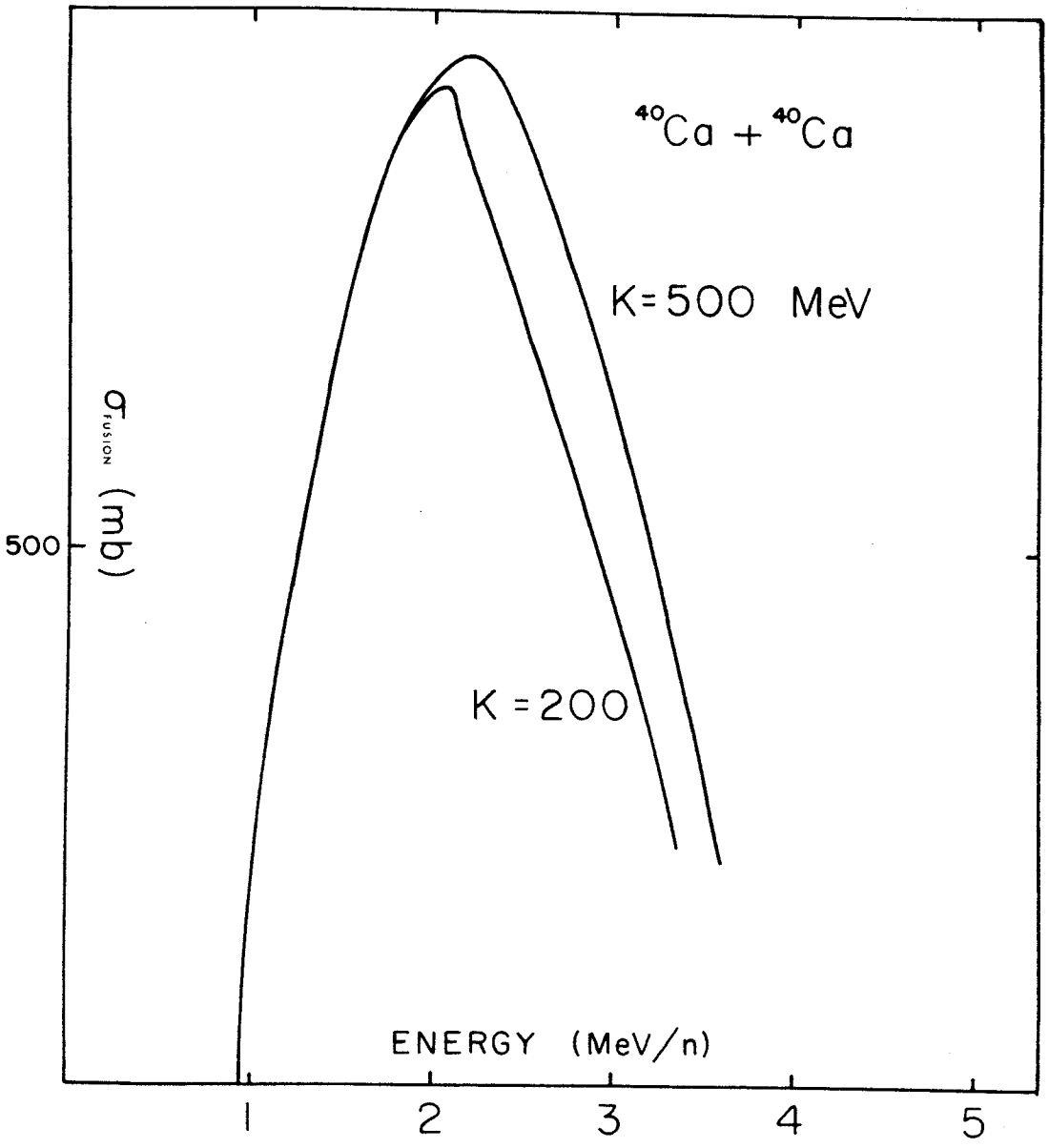

Figure 10. The cross section for the reaction $^{40}Ca(^{40}Ca,^{80}Zr)$ using two different equations of state. K = 200 MeV and K = 500 MeV represent the two extremes in compressibility.

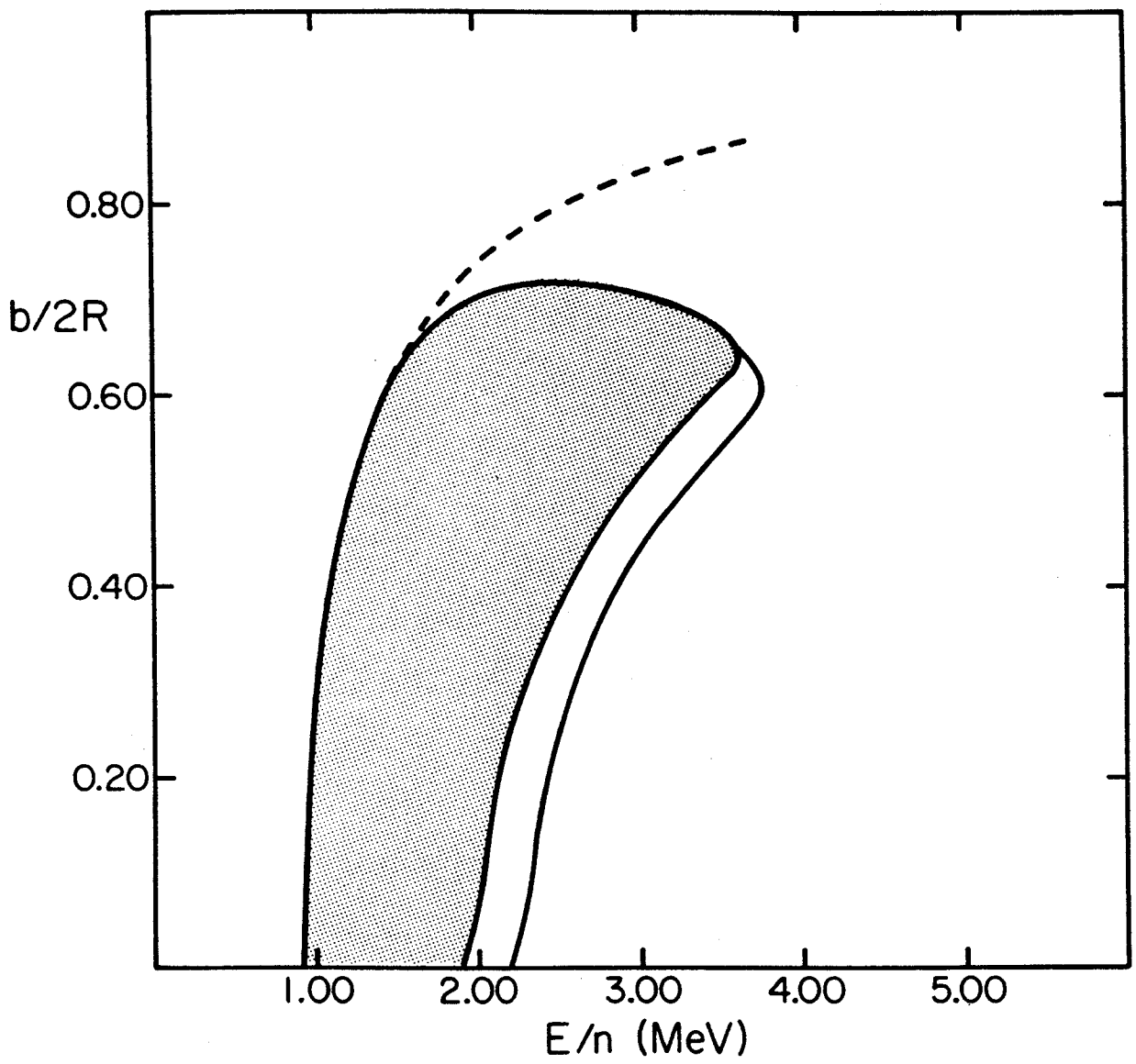

Figure 11. The fusion regime for the reaction $^{40}Ca(^{40}Ca,^{40}Ca)^{40}Ca$. The textured area represents a compressibility of K = 200 MeV. The enlarged area is for a compressibility of K = 500 MeV.

CHAPTER VIII

ANGULAR DISTRIBUTIONS

Many experiments have been done which measure the angular distribution of the products of heavy ion collisions. In describing any scattering event, the wave number k and the physical size of the system are the important parameters in determining whether the behavior is wave-like or particle-like. If $kR < 1$ a wave description is necessary. On the other hand, if $kR >> 1$, then it is valid to describe the scattering with a classical trajectory. For typical heavy ion collisions, at energies above the Coulomb barrier, $k > 10$ fm^{-1} and R is the order of 5-10 fm. For these collisions, it is valid to define an impact parameter and to describe the scattering in terms of a deflection function $\theta(b)$. The deflection function itself is not experimentally observable, but the cross section can be obtained as

$$\frac{d\sigma}{d\Omega} = \frac{b}{\sin\theta} \left|\frac{db}{d\theta}\right| .$$

An mentioned before, most of the experiments have been done at energies near the Coulomb barrier. Also, the systems tend to be asymmetric with a large target and a small projectile. Typical beams are ^{16}O, ^{20}Ne,

and ^{46}Ar. For targets, ^{208}Pb, ^{107}Ag, and ^{197}Au are commonly used. The main feature of the measured cross sections is a side peak at angles near the Coulomb grazing angle. Figure 12 shows some angular distributions for the reaction products of $^{84}Kr + ^{181}Ta$ at 3.3 MeV/nucleon.[31] For angles greater than θ_g, the cross section drops off rapidly. As the energy increases the peak moves forward and becomes sharper. This side peaking tends to support a theory which gives short interaction times, $t < 400$ fm/c. If the interaction time were long, the two nuclei would lose their individual identity. The cross section would be isotropic. This would result in a $\frac{1}{\sin\theta}$ angular distribution. Sometimes instead of a side peak the cross section decreases monotonically with increasing angle. This kind of behavior is usually associated with orbiting, or negative angle scattering.[33] There is in fact experimental evidence which indicates that negative angle scattering does occur.[34]

Figure 13 shows several time slices of a typical scattering event. The reaction is $^{118}Pd + ^{118}Pd$. The energy, in the center of mass frame, is 5 MeV/nucleon. The impact parameter is .4 R, which gives an initial orbital angular momentum of L = 130 h. After impact the compound system goes through compression, decompression, and then a rarefaction, during which a neck region

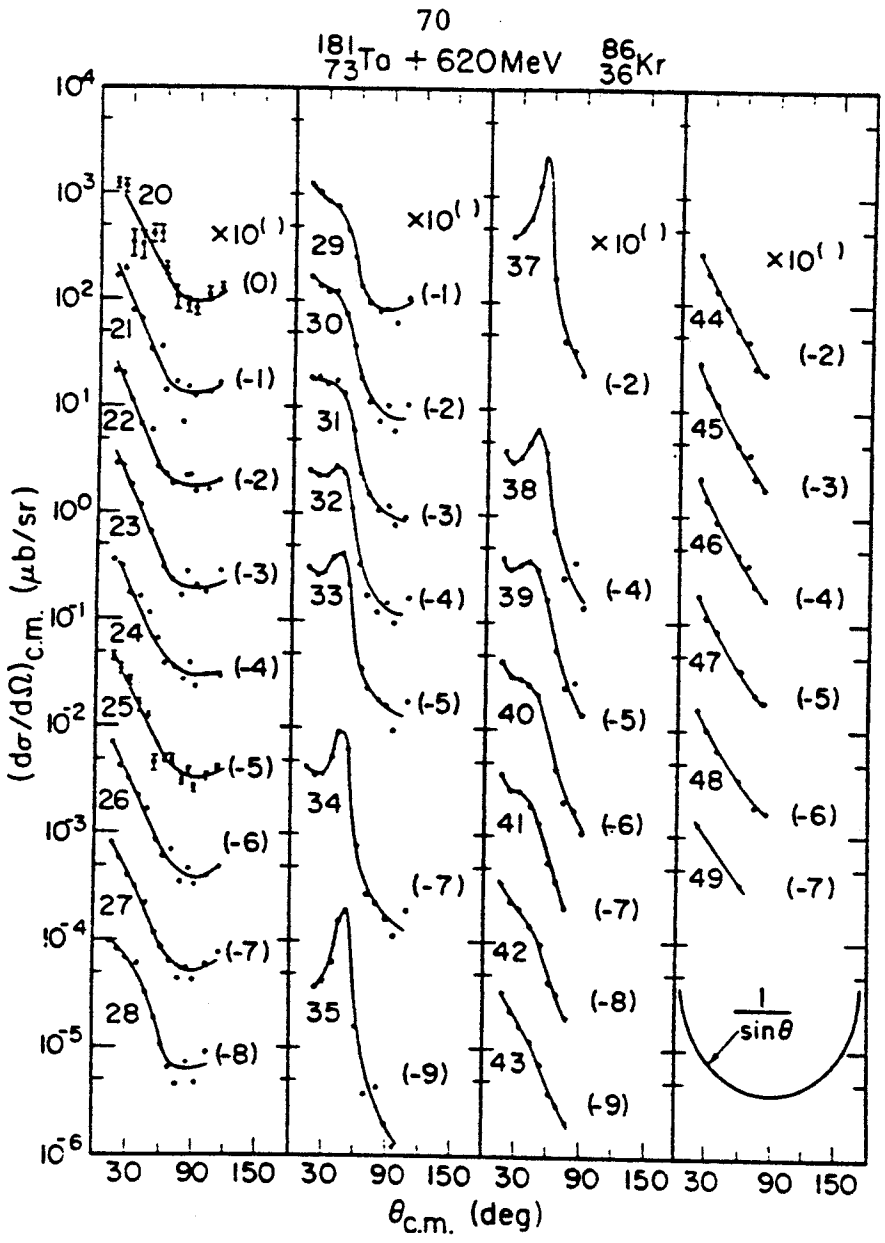

Figure 12. Angular distributions for the reaction products of the collision between 620 MeV ^{86}Kr ions and a ^{181}Ta target.

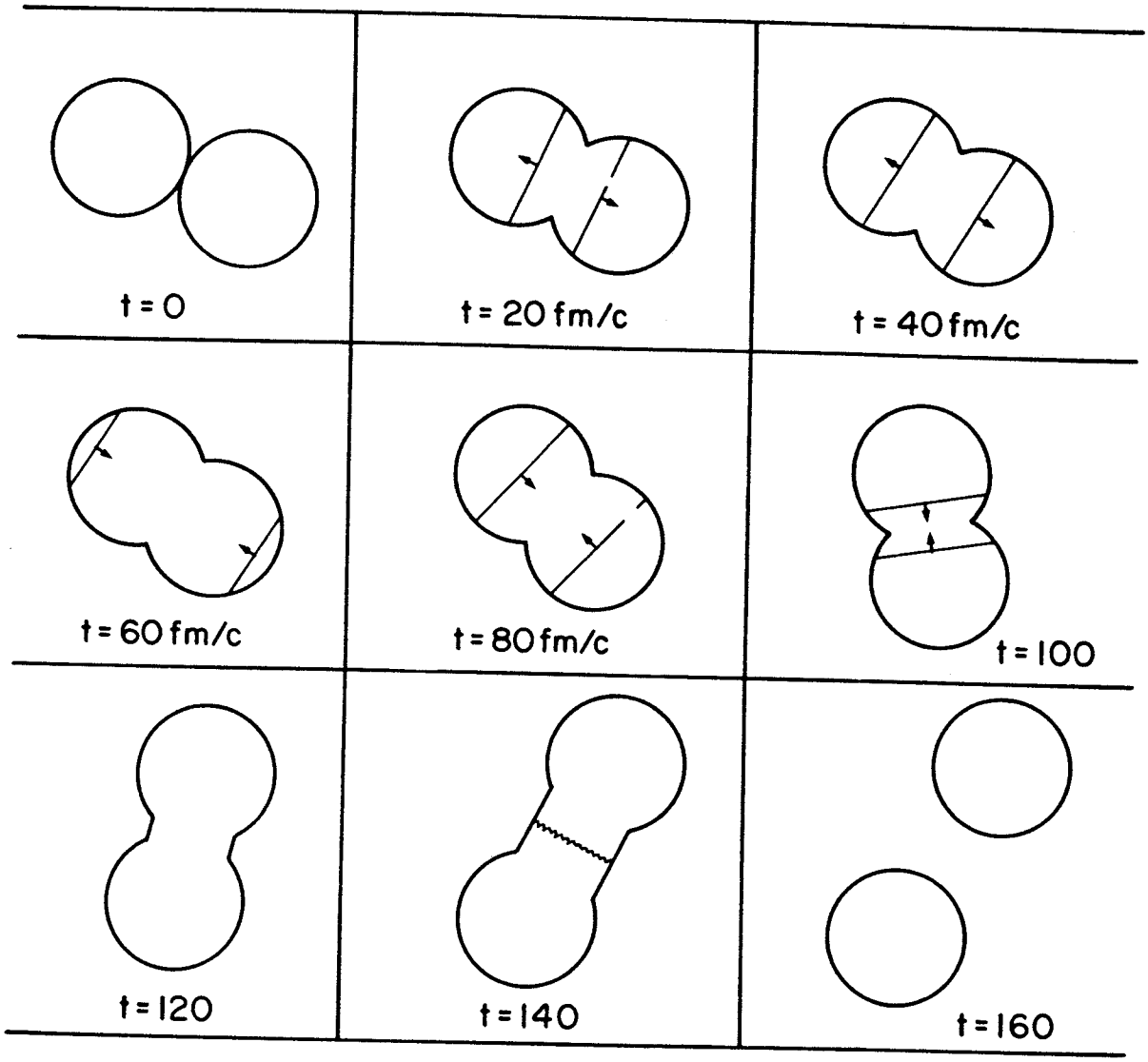

Figure 13. Collision between two ^{118}Pd nuclei at an energy of 5 MeV/n (c.m.). The straight line represents the boundary between the two zones. The small arrows indicate its direction of motion.

is formed. The rarefied region causes a negative pressure which slows down the outward motion. At t = 140 fm/c the neck snaps. The energy that had gone into creating the rarefied region now goes into large collective vibrations in the outgoing nuclei. The energy lost to friction is about 1 MeV/nucleon, and the energy in the vibration is also about 1 MeV/nucleon. The relative kinetic energy has thus been reduced to about 3 MeV/nucleon. The angle at which scission occurs is ϕ = 104 degrees. From this point the scattered particle follows a Coulomb trajectory with an assymptotic angle at θ = 46 degrees. Because of the tangential friction the orbital angular momentum in the outgoing channel has been reduced to 94 h.

Figures 14, 15, and 16 show families of deflection functions for energies in the range from just above the Coulomb barrier to 5 MeV/nucleon. Most of the features of these curves have been discussed in previous sections. The large impact parameters $b > b_g$ correspond to elastic Coulomb scattering. As b decreases below the grazing value the deflection function is pulled to more forward angles by the nuclear interaction. The peak in the deflection function at $b = b_g$ is sometimes called the Coulomb rainbow. This is associated with a peak in the cross section, for the nearly elastic scattering events,

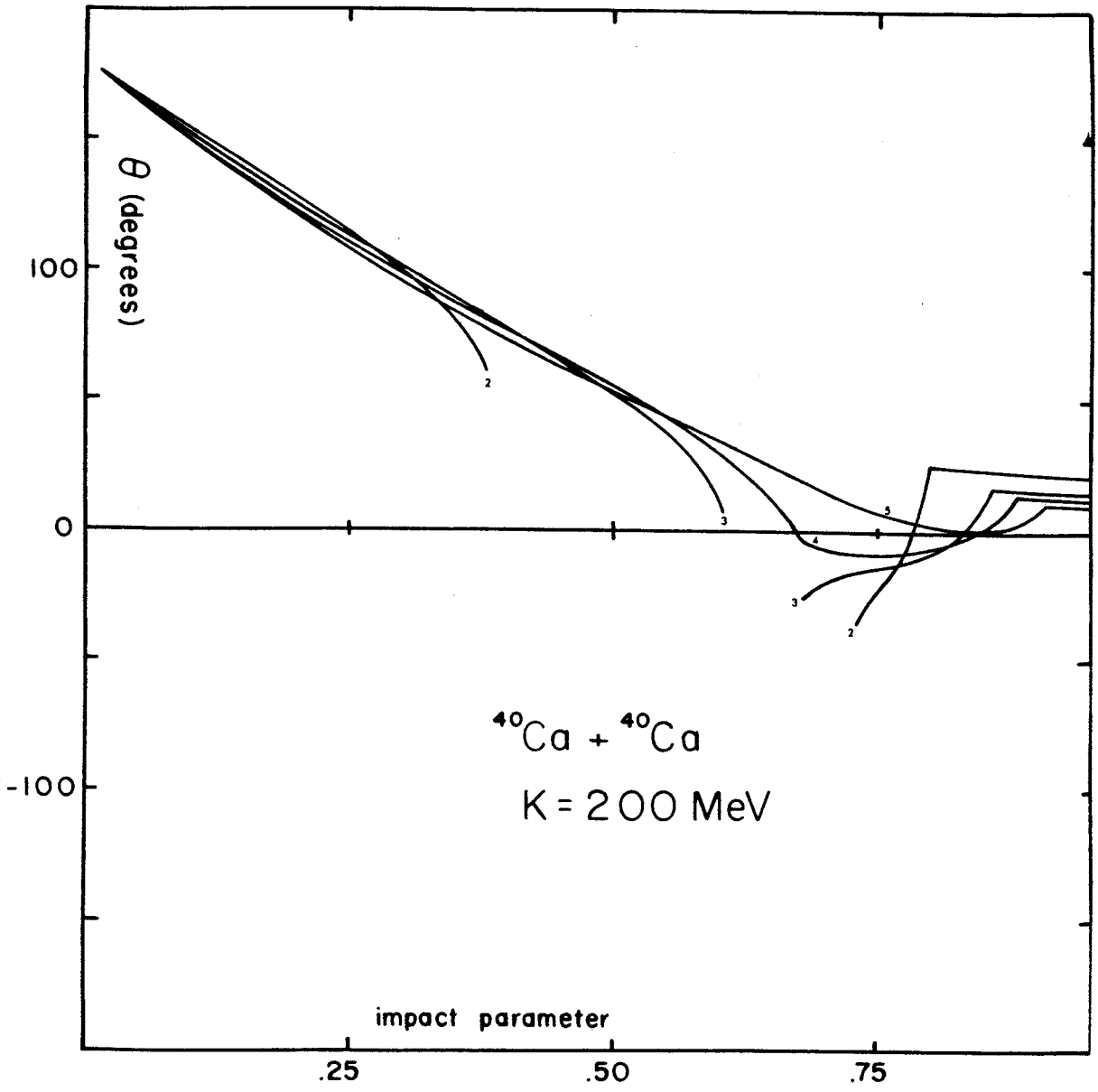

Figure 14. Deflection function θ(b) for the collision between two Calcium nuclei. The small numbers indicate the center of mass energy in MeV/n.

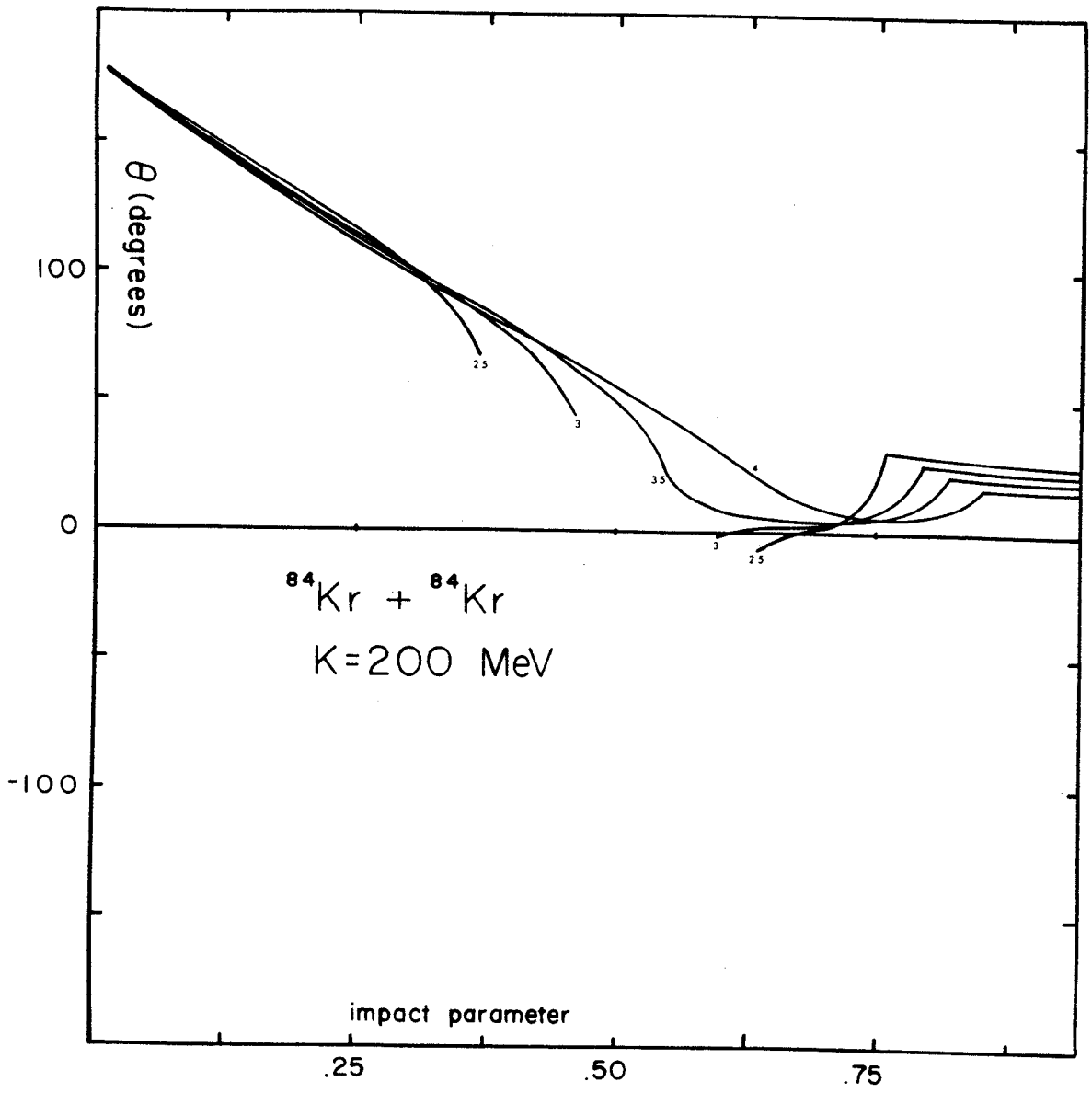

Figure 15. Deflection function for the reaction $^{84}Kr(^{84}Kr,^{84}Kr)^{84}Kr$. The compressibility is K = 200 MeV. The small numbers indicate the center of mass energy in MeV/n.

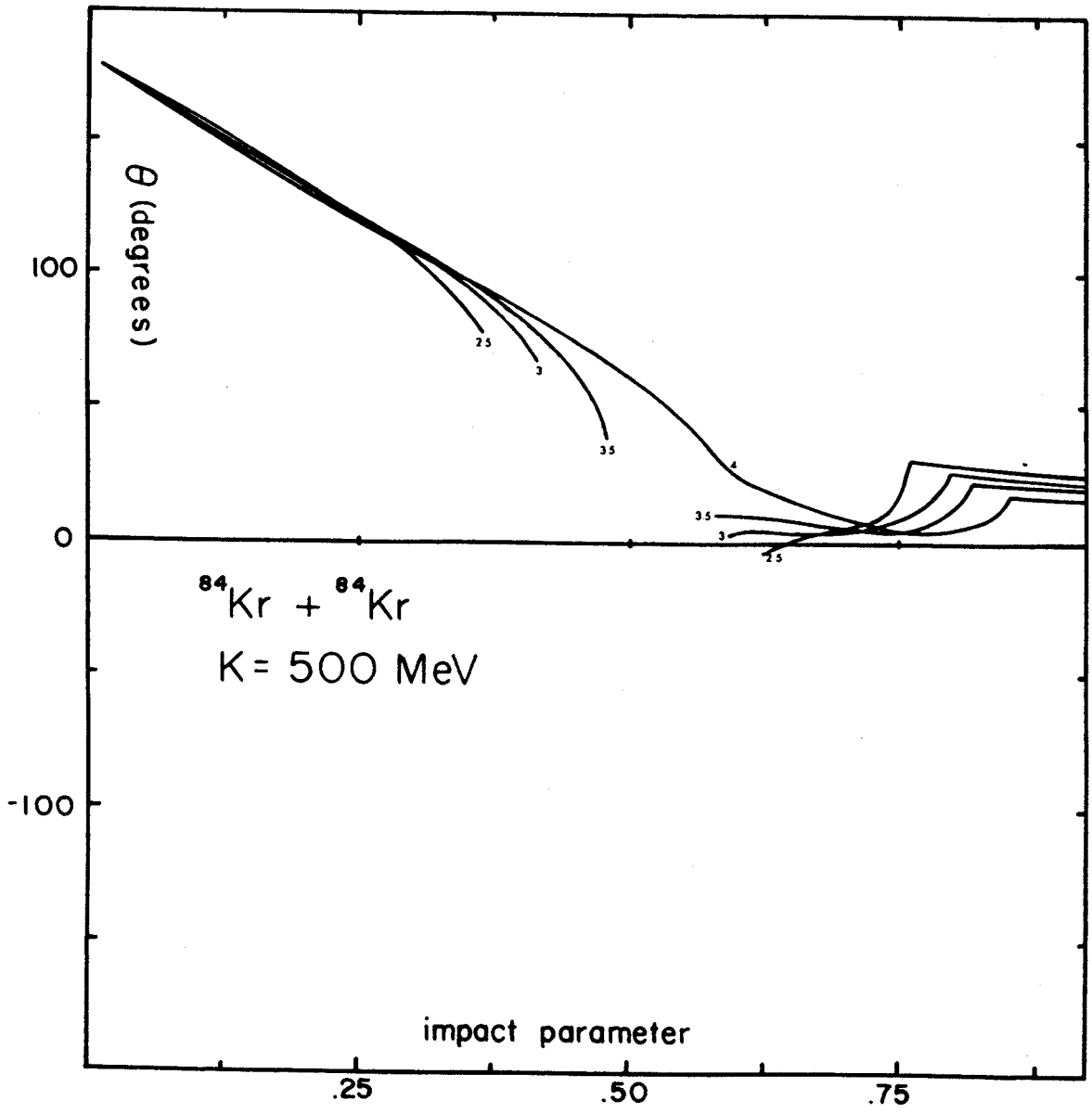

Figure 16. The deflection function for the reaction $^{84}Kr(^{84}Kr,^{84}Kr)^{84}Kr$ using the K = 500 MeV equation of state. The small numbers indicate the center of mass energy in MeV/n.

at the Coulomb grazing angle. In our model there is no Coulomb rainbow because of the discontinuous nature of the surface tension. The deflection function flattens out again at more forward angles. This gives a peak in the cross section for the deeply inelastic events. Figure 14 shows a family of curves for the nuclear system $^{40}Ca + {}^{40}Ca$. In this case the deep inelastic peak occurs at a negative angle. In Figure 15 the reaction $^{84}Kr + {}^{84}Kr$ is shown. Comparing these two cases shows how the angular distribution changes as the size of the nucleus increases. The most noticeable effect is that the strongly damped peak moves toward more positive angles. This result can be understood by considering how the forces change with nuclear size. The surface tension goes like $A^{1/3}$. The cohesive force increases as $A^{2/3}$, as does the centrifugal force. The Coulomb repulsion varies like $A^{4/3}$. As the nucleon number increases the Coulomb plus centrifugal force increases faster than the attractive forces. Because of this, the breakup will occur more quickly for the larger system, and there will be less tendency to orbit and scatter to negative angles. In Figure 16 are the results for the same system, $^{84}Kr + {}^{84}Kr$, using a different equation of state. The compressibility for this case

is 500 MeV. The most noticeable difference is an increase in the fusion regime. The nuclear rainbow does not appear to depend much on the equation of state.

CHAPTER IX

EVALUATION OF RESULTS

In comparing the predictions of this model with the results of experiment we find fairly good agreement in some areas and poor agreement in others. Regarding energy loss, one would expect from the results of experiment to find large energy losses for any collision in which the colliding nuclei interpenetrate deeply. The results of our model agree with this up to the low impact parameters, but the energy loss suffered during head-on collisions is not as great as would be expected. Further development of this model must include a mechanism by which energy can be dissipated from the radial motion. Taking into account the relaxation of the stress tensor due to nucleon-nucleon collisions will account for some energy loss. Also, by allowing a more general velocity field in the compressed region, we would expect the collective motion to become more randomized. Both of these improvements would increase the energy loss at low impact parameters. To gain some insight as to the size of these effects a calculation was done in which the stress tensor was allowed to relax from the elastic form to the fluid form in the following way.

$$S_{ij} = S_{ij}^{fluid} + e^{-t/\tau} [S_{ij}^{elastic} - S_{ij}^{fluid}]$$

The relaxation time was taken to be $\tau = \frac{1000}{E_n}$ fm/c. This is based on a calculation of the collision rate in an infinite Fermi system having a deformed Fermi surface, in the limit of small deformations.[42] The results are shown in Figure 17 along with the standard results discussed earlier. It is clear from the figure that the scattered products have less energy. This is because for a given density the pressure decreases as S_{ij} relaxes toward the fluid model. Now there is less pressure during the decompression stage than during the compression stage. Using this form for S_{ij} will also change the fusion cross section. The results are presented for comparison in Figure 18. The effect is not large, but at low impact parameters the energy range for fusion is increased by about 10%. The fusion cross sections calculated using this compressible fluid model are quite consistent with the results of experiments. Many more experiments must be done, using larger nuclei and higher energies, before a complete picture of fusion can be presented. Figure 19 shows the data from an experiment done with $^{16}O + ^{26}Mg$. Cross sections were measured at various energies up to about 4 MeV/nucleon.[36] The solid curve is from a calculation made using the simplified

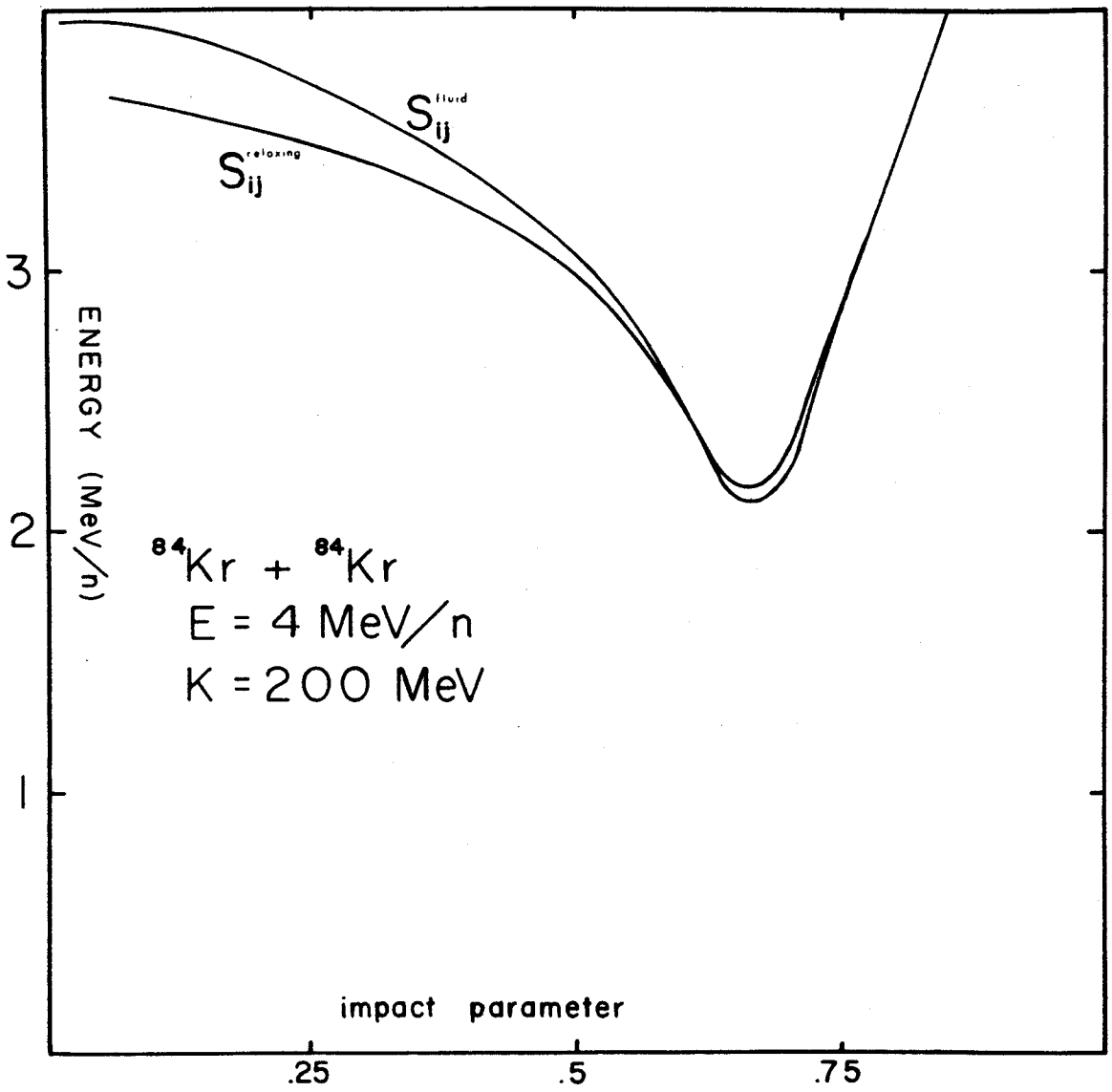

Figure 17. A comparison of the energy loss functions using two different forms for the stress tensor.

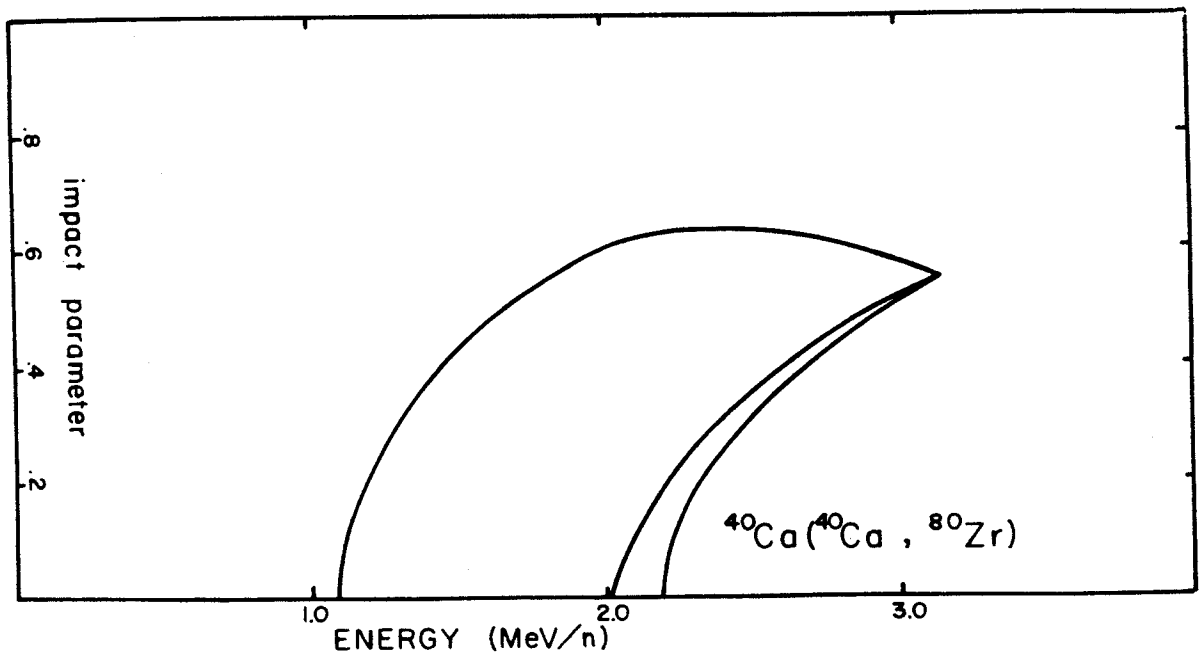

Figure 18. The effect of the relaxing stress tensor on the fusion regime.

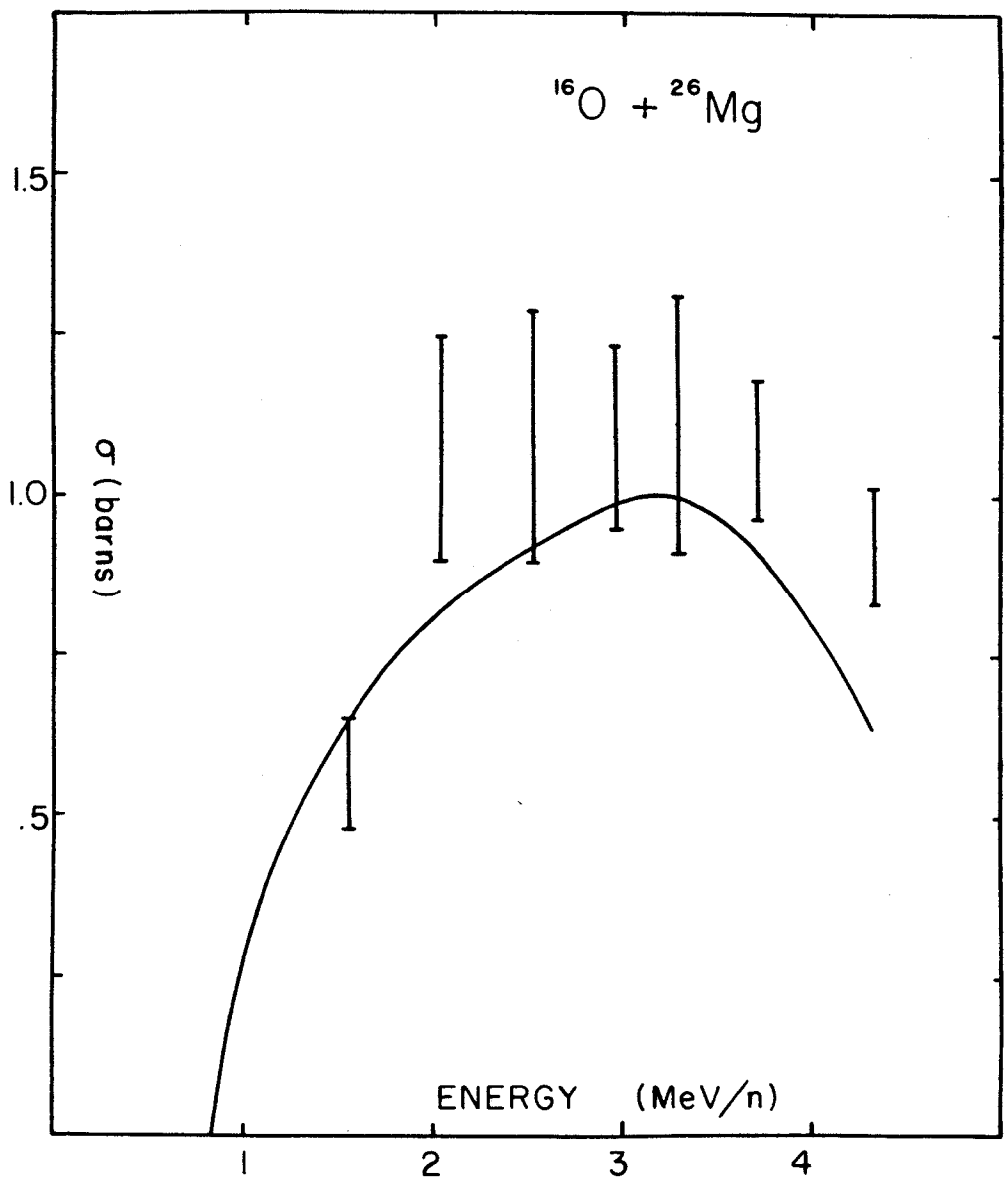

Figure 19. A comparison of the experimental results of Reference 36 with the predicted results of the simple model described in Chapter VIII.

model for fusion in which friction was neglected. The agreement with experiment is quite good. The low cross sections predicted at the higher energies will increase when the tangential friction is included. Our model, of course, predicts no cross section for fusion at energies below the Coulomb barrier. Experiments do show a small but finite cross section for energies slightly below V_c. Experiments done with $^{10}B + ^{14}N$ have shown measurable cross sections for fusion at energies down to .25 MeV/nucleon below the Coulomb barrier.[35] This corresponds to an interaction radius of about twice the mass radius. For these events the model we have described is not adequate. Several other experiments have also been analyzed, and agreement is quite good at the low energies.[30] At the higher energies the predicted fusion cross sections are somewhat smaller than the measured values. This would seem to indicate that there are other mechnisms by which energy is dissipated.

It is difficult to compare the angular distributions predicted by our model directly with experimental data but some general comparison can be made. Typical data shows either a monotonically decreasing cross section as the angle increases, or a side peak at angles near to, or somewhat forward of, the grazing angle. From the results presented in Figures 14, 15, and 16 one can

clearly see the side peak in the deflection function. However, it is at an angle considerably forward of the Coulomb grazing angle. For $^{40}Ca + ^{40}Ca$ the peak is at about 10 degrees. For the reaction $^{84}Kr + ^{84}Kr$ the side peak is even more forward at about 5 degrees.

CHAPTER X

A COMPARISON OF THE RESULTS WITH THE OTHER MODELS

In comparing the results of the compressible fluid drop model with the other calculations that have been done, it should first be noted that there are some fundamental differences. One example of this is the existence of an angular momentum window in the fusion cross section. This is a characteristic predicted by some of the models and not by others. Another example of a basic difference is the kind of scattering rainbow predicted by the model. In the following discussion we will consider each aspect of heavy ion collisions and briefly describe what the various models have to say about it.

First of all consider the energy loss. In the classical friction model of Gross and Kalinowski[7] the colliding nuclei undergo a rapid energy loss as a result of a large radial friction. Similarly, in the TDHF calculations and in the surface excitation model, the energy of the scattered particle decreases as the impact parameter decreases. Other than an understandable dip near the fusion regime, this decrease is monotonic. In

Figure 20 a comparison is shown between our results and a TDHF calculation done by another group.[4] The energy was chosen to give the same low ℓ window size. The results are comparable, however, the TDHF calculation does not exhibit any elastic bouncing at low impact parameters as is characteristic of our results.

The next aspect of heavy ion reactions we will discuss is fusion. In this area the TDHF calculations are in good agreement with our results. Using a TDHF method, the reaction $^{118}Pd + ^{118}Pd$ at an energy of 1.35 MeV/nucleon has been studied by Cusson and co-workers.[3] The equations of motion were solved for several values of the impact parameter. In this calculation it was found that for b less than .27 the system remained fused. In our calculation we found fusion for an impact parameter of less than .33. This number is critically dependent on what value is taken for the interaction radius and so we consider this to be in good agreement. An example of a very large system is the reaction $^{208}Pb + ^{208}Pb$. The energy here is also only slightly above the Coulomb barrier. This result illustrates the effect of the Coulomb repulsion on fusion. Fusion does not occur even at zero impact parameter. Figure 21 shows the relative separation of the two nuclei as a function of time in a head-on collision. One curve

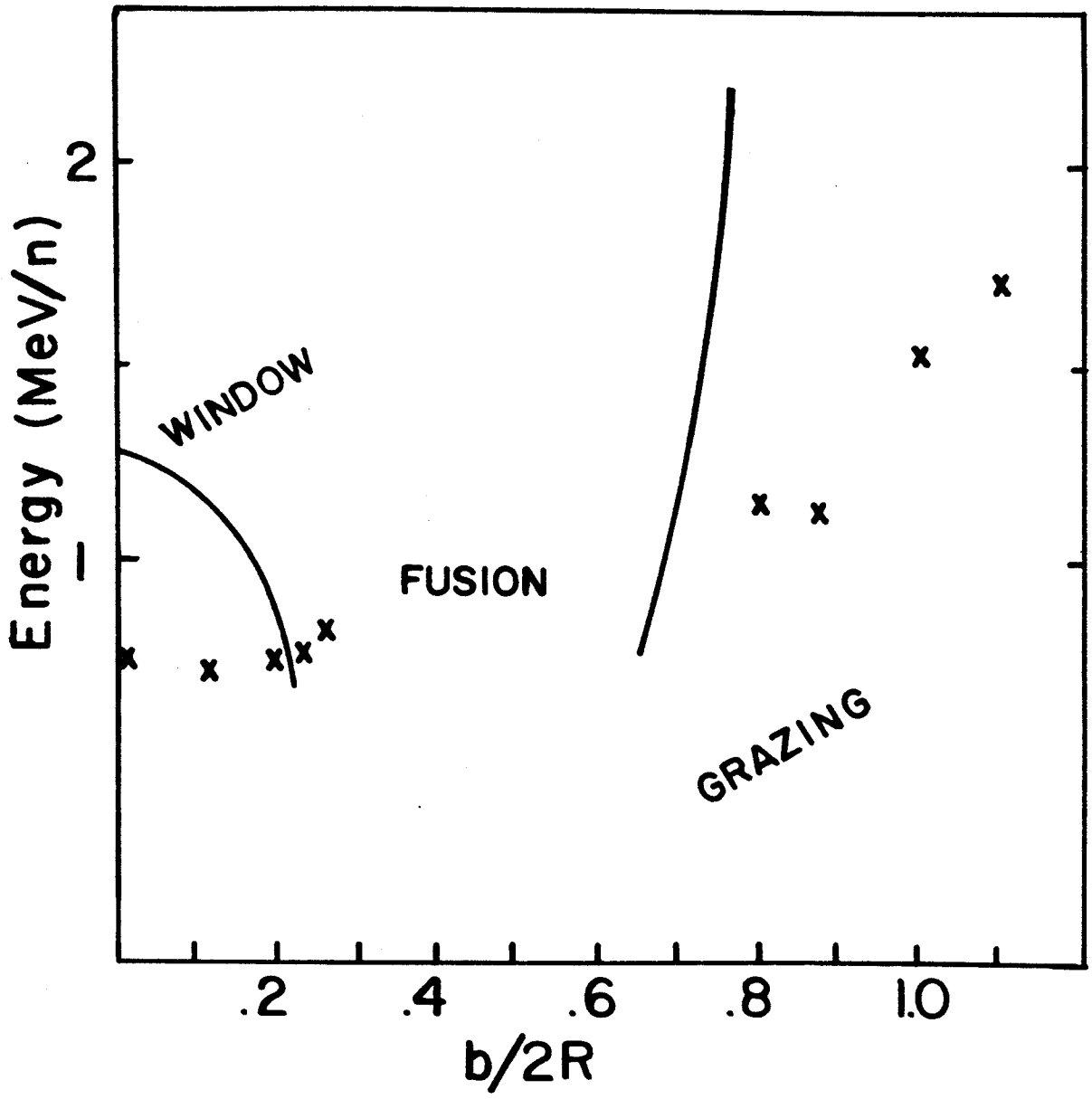

Figure 20. Final state energies in the reaction $^{40}Ca(^{40}Ca,^{40}Ca)^{40}Ca$. The Coulomb barrier in our model is at .85 MeV/n. The incident energy in the TDHF study is 1.738 MeV/n. To keep the same window we use an energy of 2.1 MeV/n.

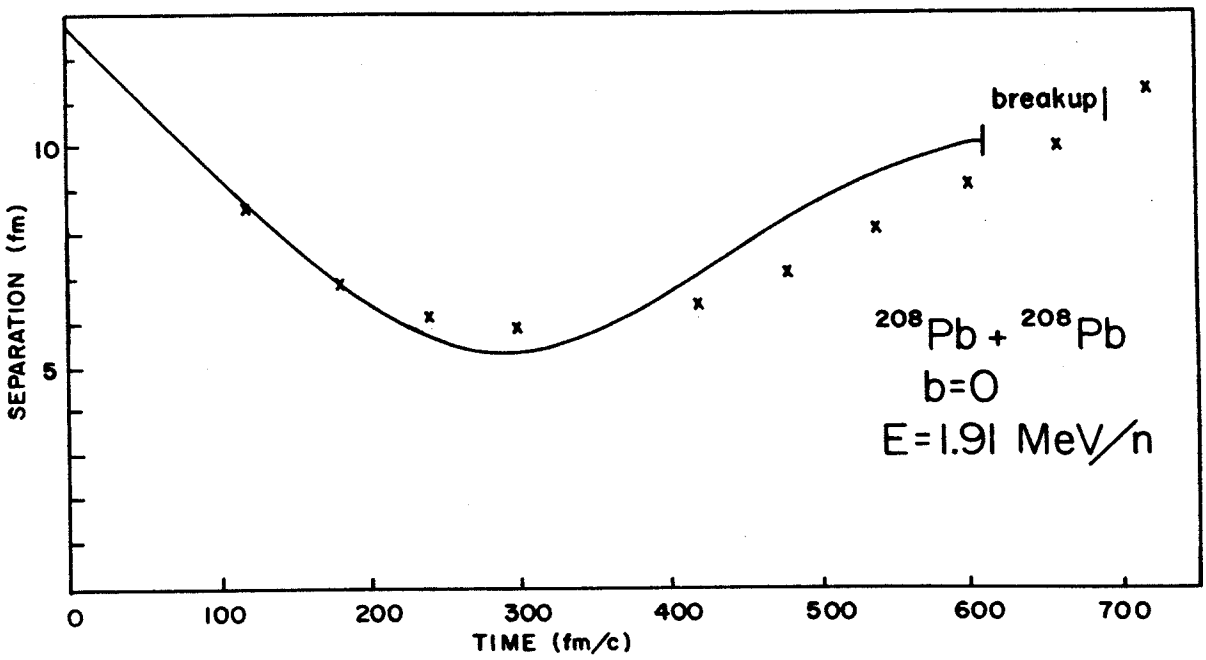

Figure 21. The distance between centers of two Pb nuclei as a function of time. The line at the end indicates breakup. The solid line is our calculation and the x's are from the TDHF calculations of Reference 4.

represents the TDHF result, the other is from the compressible fluid drop model. At somewhat higher energies another TDHF calculation was done for the reaction $^{40}Ca + ^{40}Ca$. In this case the energy was 1.738 MeV/nucleon, or about .82 MeV/nucleon above the Coulomb barrier. These workers found that there was an angular momentum window in which fusion occurred. This feature is also present in our model at slightly higher energies. In terms of the impact parameter they found that the system remained fused if b was in the range from .17 to .46. For impact parameters outside this window, a scattering event takes place. This fusion window is also present in the surface excitation model.

The results of a calculation done by Broglia and others are shown in Figure 22. The cases presented in this study represent energies in the range from 3 to 6 MeV/nucleon above the Coulomb barrier. The fusion window is quite small and sits around b/2R = .5. Looking more closely at the results for the reaction Ar + Ag we find that at 5.24 MeV/nucleon the window is between b/2R = .43 and b/2R = .59. At the highest energy 6.98 MeV/nucleon the window lies between b/2R = .52 and b/2R = .59. This behavior is consistent with the expected decrease in fusion cross section as the energy

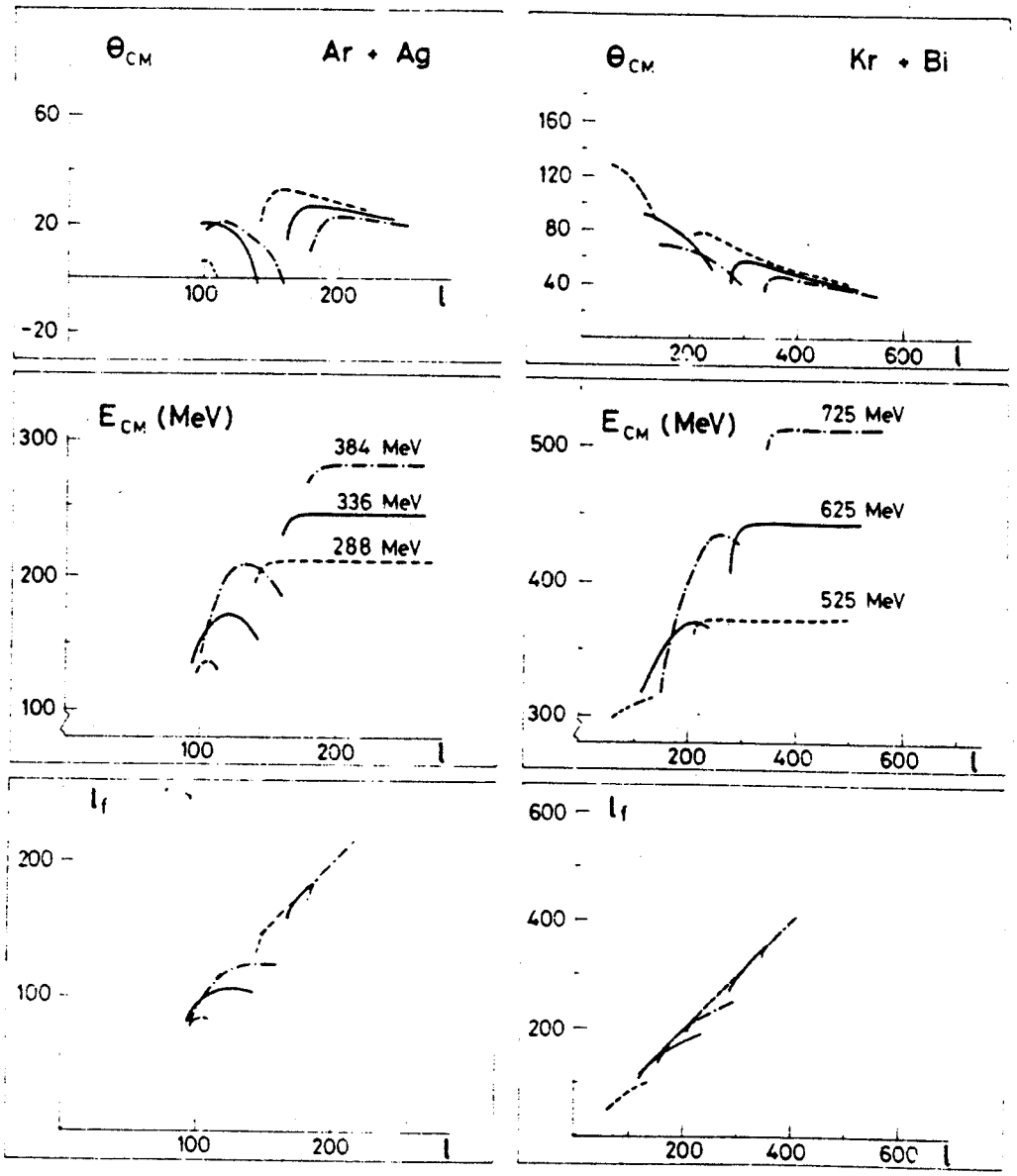

Figure 22. Results of a calculation done using a surface excitation model as described in Reference 11.

increases. For any impact parameter one can calculate the distance of closest approach on the Coulomb trajectory. If we do this for the largest impact parameter in the fusion regime, we find that the distance of closest approach ranges between .8 and .9 times the mass radius. The penetration depth required increases as the energy increases. It is also interesting to calculate the radial velocity at the point of impact using the lower impact parameter. In all cases this velocity is between .065 c and .075 c. This suggests that the radial velocity at the point of impact is an important parameter in determining whether or not the system fuses. In the friction model this fusion window is not present. All trajectories with angular momentum less than some critical value L_{cr} will lead to fusion. This is also the case for the incompressible fluid model. This model has been used by Nix and Sierk to calculate fusion cross sections.[8] Their results show a smaller cross section than ours with a peak at about .5 MeV/nucleon above the Coulomb barrier. It should be noted that in this calculation there was no dissipation.

The final topic we will consider is the angular distribution. In our model this is dominated by a nuclear rainbow which appears at an angle more forward than the Coulomb grazing angle. This peak is made up

of reaction products that have suffered a considerable energy loss. Both the friction model and the surface excitation model exhibit a Coulomb rainbow. This appears near the grazing angle and consists of nuclei that have been scattered with very little loss of energy. The TDHF calculations should be able to predict angular distributions. However, because of the length of the calculation, there is not enough information to construct a deflection function. In Table 3 we present a summary of the results of the various models that have been considered.

Table 3. A summary of the various models which have been used to describe heavy ion collisions.

	Energy Loss	Fusion	Angular Distribution
Friction model of Gross and Kalinowski	Large radial friction causes a rapid energy loss.	All angular momenta between 0 and L_{cr} lead to fusion.	Exhibits a Coulomb rainbow of nearly elastic collisions at $\theta \simeq \theta g$.
TDHF	Energy of the scattered particle decreases as b gets smaller.	Fusion cross section peaks at about 1 MeV/n above V_c. At higher energy there is an angular momentum window.	Not enough data.
Surface excitation model of Broglia et al.	Energy loss increases as the impact parameter gets smaller.	Has an angular momentum window at 2-4 MeV/n	Coulomb rainbow at $\theta \simeq \theta g$. No nuclear rainbow.
Incompressible fluid model of Nix and Sierk	No energy loss.	Relatively small cross sections, peaked at about 5 MeV/n above V_c. $\sigma \simeq 1/3$ barn.	Scattering is not discussed.
Compressible fluid model.	Energy loss increases as b goes for b_g to $b \simeq .4$. Head-on collisions are more elastic.	Cross sections of about 1 barn, peaks at 2 MeV/n above V_c. Angular momentum window up to 4 MeV/n.	No Coulomb rainbow. Has a nuclear rainbow of strongly damped events at $\theta < \theta g$.

LIST OF REFERENCES

LIST OF REFERENCES

1. T.D. Lee, Rev. Mod. Phys. 47 (1975) 267.
2. S. Koonin et al., Phys. Rev. C15 (1977) 1359.
3. R.Y. Cusson and H.W. Meldner, Phys. Rev. Lett. 42 (1979) 694.
4. H. Flocard and M.S. Weiss, Phys. Rev. C18 (1978) 573.
5. A.K. Dhar and B.S. Nilsson, Phys. Lett. 77B (1978) 50.
6. A.K. Dhar, Phys. Rev. Lett. 42 (1979) 1142.
7. D. Gross and H. Kalinowski, Phys. Report 45C (1978) 175.
8. J.R. Nix and A.J. Sierk, Phys. Rev. C15 (1977) 2072.
9. K.T.R. Davies et al., Phys. Rev. C13 (1976) 2385.
10. R.A. Broglia et al., Phys. Lett. 53B (1974) 301.
11. R.A. Broglia et al., Phys. Lett 61B (1976) 113.
12. H. Esbensen et al., Phys. Rev. Lett. 41 (1978) 296.
13. E. Wigner, Phys. Rev. 40 (1932) 749.
14. J. Negele and D. Vautherin, Phys. Rev. C5 (1972) 1472.
15. A. Vlasav, J. Phys. (USSR) 9 (1945) 25.
16. D. Youngblood et al., Phys. Rev. Lett. 39 (1977) 1188.
17. F. Reif, Fundamentals of Statistical and Thermal Physics. New York: McGraw-Hill, 1965.

18. Ya.B. Zel'dovich and Yu.P. Raizer, Elements of Gas Dynamics. New York: Academic Press, 1966.

19. L.D. Landau and E.M. Lifshitz, Fluid Mechanics. New York: Pergamon, 1959.

20. D. Goodstein, States of Matter. Reading: Addison-Wesley, 1950.

21. K. Huang and C.N. Yang, Phys. Rev. 105 (1957) 767.

22. W. Myers and W. Swiatecki, Ann. Phys. 55 (1969) 395.

23. D. Vautherin and D. Brink, Phys. Rev. C5 (1972) 626.

24. L. Zamick, Phys. Lett. 45B (1973) 313.

25. L. Thomas, Proc. Cambridge Phil. Soc. 23 (1927) 542.

26. H. Goldstein, Classical Mechanics. Englewood Cliffs: Prentice-Hall, 1975.

27. G. Bertsch and D. Mundinger, Phys. Rev. C7 (1978) 1646.

28. H. Enge, Introduction to Nuclear Physics. Reading: Addison-Wesley, 1966.

29. F. Hanappe et al., Phys. Rev. Lett. 32 (1974) 738.

30. J.R. Birklund et al., UR-NSRL-193 submitted to Phys. Reports.

31. B. Cauvin et al., Nucl. Phys. A294 (1978) 225.

32. J.N. De, Phys. Lett. 66B (1977) 315.

33. J. Wilczynski, Phys. Lett. 47B (1973) 484.

34. W. Trautman et al., Phys. Rev. Lett. 39 (1977) 1062.

35. Shiu-Chin Wu et al., Nucl. Phys. A312 (1978) 177.

36. D. Horn et al., Nucl. Phys. A313 (1978) 238.

37. C.Y. Wong et al., Nucl. Phys. A253 (1975) 469.

38. N. Bogoliubov and K. Gurov, J. Exp. Theo. Phys. (USSR) 17 (1947) 614.

39. M. Redlich, Phys. Rev. 99 (1955) 1421.

40. A. Fetter and J. Walecka, Quantum Theory of Many-Particle Systems. New York: McGraw-Hill, 1971.

41. K.A. Brueckner et al., Phys. Rev. 95 (1954) 217.

42. G. Bertsch, Z. Physik A289 (1978) 103.

43. M. Golin and L. Zamick, Nucl. Phys. A295 (1975) 320.

44. G. Bertsch, Ann. Phys. 86 (1974) 138.

45. J. Huizenga et al., Phys. Rev. Lett. 37 (1976) 885.